Reactive Geochemical Transport Simulation to Study Mineral Trapping for CO_2 Disposal in Deep Saline Arenaceous Aquifers

Tianfu Xu, John A. Apps, and Karsten Pruess

Earth Sciences Division, Lawrence Berkeley National Laboratory, University of California, Berkeley, CA 94720, USA

Abstract. A reactive fluid flow and geochemical transport numerical model for evaluating long-term CO_2 disposal in deep aquifers has been developed. Using this model, we performed a number of sensitivity simulations under CO_2 injection conditions for a commonly encountered Gulf Coast sediment to analyze the impact of CO_2 immobilization through carbonate precipitation. Geochemical models are needed because alteration of the predominant host rock aluminosilicate minerals is very slow and is not amenable to laboratory experiment under ambient deep-aquifer conditions. Under conditions considered in our simulations, CO_2 trapping by secondary carbonate minerals such as calcite ($CaCO_3$), dolomite ($CaMg(CO_3)_2$), siderite ($FeCO_3$), and dawsonite ($NaAlCO_3(OH)_2$) could occur in the presence of high pressure CO_2. Variations in precipitation of secondary carbonate minerals strongly depend on rock mineral composition and their kinetic reaction rates. Using the data presented in this paper, CO_2 mineral-trapping capability after 10,000 years is comparable to CO_2 dissolution in pore waters (2-5 kg CO_2 per cubic meter of formation). Under favorable conditions such as increase of the Mg-bearing mineral clinochlore ($Mg_5Al_2Si_3O_{10}(OH)_8$) abundance, the capacity can be larger (10 kg CO_2 per cubic meter of formation) due to increase of dolomite precipitation. Carbon dioxide-induced rock mineral alteration and the addition of CO_2 mass as secondary carbonates to the solid matrix results in decreases in porosity. A maximum 3% porosity decrease is obtained in our simulations. A small decrease in porosity may result in a significant decrease in permeability. The numerical simulations described here provide useful insight into sequestration mechanisms, and their controlling conditions and parameters.

Key words. CO_2 sequestration, CO_2 disposal, numerical simulation, mineral trapping, deep saline aquifer, reactive geochemical transport, Gulf Coast sediments, natural diagenesis.

TABLE OF CONTENTS

1. Introduction

A reduction in the release rate of carbon dioxide (CO_2) to the atmosphere is considered an essential first step in the control of global warming. One way of achieving this is to dispose of CO_2 in structural reservoirs in deep permeable geologic formations, (Holloway, 1997). Such formations could include aquifers, oil and gas fields, and coal seams. Aquifers are the most abundant fluid reservoirs in the subsurface. The deepest aquifers in the United States usually contain brackish or saline water. Aquifers exceeding 10,000 mg/L (TDS: total dissolved solids) are excluded by the U.S. Environmental Protection Agency as underground sources of drinking water. Hence, they are logical targets for the eventual disposal of CO_2. The feasibility of storing CO_2 in aquifers has been discussed in the technical literature over the last decade. Studies include an evaluation of the feasibility of CO_2 aquifer storage in The Netherlands (Lohuis, 1993) and in the Alberta Basin, Canada (Gunter et al., 1993; Bachu et al., 1994; Law and Bachu 1996; Gunter et al., 1996 and 1997). Furthermore, large-scale CO_2 disposal in an aquifer is already being practiced in the Norwegian sector of the North Sea (Korbol and Kaddour, 1995).

Long-term sequestration of CO_2 raises new scientific challenges (Rudnicki and Wawersik, 1999), particularly in the fields of hydrogeology, geochemistry, geophysics, and geomechanics. These challenges must be addressed before this technology can be implemented safely, efficiently, and predictably. In this paper, we focus our attention on geochemical issues arising from aquifer CO_2 disposal.

Carbon dioxide is retained in geologic formations in three ways (Hitchon, 1996). First, CO_2 can be trapped as a gas or supercritical fluid under a low-permeability caprock.

This process, commonly called hydrodynamic trapping, will likely be, in the short term, the most important mechanism of retention. Second, CO_2 can dissolve into the groundwater, referred to as a solubility trapping. The dissolution of CO_2 in groundwater increases the acidity of water and affects the solubilities of minerals composing the host rock matrix. Third, CO_2 can react directly or indirectly with minerals and organic matter in the geologic formation leading to the precipitation of secondary carbonates and the solubilization of organic matter. The former process, so-called "mineral trapping", is potentially attractive because it could immobilize CO_2 for long time scales, and prevent its easy return to the atmosphere. The interaction of CO_2 with alkaline aluminosilicate minerals will also result in the formation of soluble carbonates and bicarbonates in solution, thereby enhancing "solubility trapping".

The appealing concept that CO_2 could be permanently sequestered as carbonates in the subsurface environment by mineral trapping (Bachu et al., 1994; Ortoleva, 1998) has prompted experimental studies in Europe (Pearce et al., 1996; Rochelle et al., 1996) and Canada (Gunter et al., 1997) to investigate this process.

Numerical modeling of geochemical processes is a necessary tool for long-term CO_2 disposal in deep aquifers, because alteration of the predominant host rock aluminosilicate minerals is very slow and is not experimentally accessible under ambient deep-aquifer conditions. Xu et al. (2001) performed batch geochemical modeling for three different aquifer mineralogies in the presence of CO_2 at high pressure. The modeling considered (1) redox processes that could be important in deep subsurface environments, (2) the presence of organic matter, (3) the kinetics of chemical interactions between the host rock minerals and the aqueous phase, and (4) CO_2 solubility dependence

on pressure, temperature and salinity of the system. The geochemical evolution under both natural background and CO_2 injection conditions was evaluated. Their results indicate that CO_2 sequestration by matrix minerals varies considerably with rock type. Under favorable conditions the amount of CO_2 that may be sequestered by precipitation of secondary carbonates is comparable with and can be larger than the effect of CO_2 dissolution in pore waters. The first rock type previously investigated is a mineral assemblage representative of a glauconitic sandstone aquifer from the Alberta Sedimentary Basin (Gunter et al., 1997). The second rock type evaluated was a proxy for a sediment from the United States Gulf Coast (Apps, 1996). The third rock type investigated in the prior study was dunite, an essentially monomineralic rock consisting of olivine. This rock is a mantle residue after depletion of basaltic magma, and occurs rarely at the earth's surface. It has a very large CO_2 sequestration capacity.

For large-scale injection of CO_2 into aquifers, geochemical processes are strongly affected by physical processes such as multiphase fluid flow and solute transport. Fluid pressures will rise as CO_2 displaces aquifer water in which it partly dissolves. The dissolution of primary and precipitation of secondary minerals change formation porosity and permeability, and may alter patterns of fluid flow. All processes involving coupled hydrologic and chemical effects influence the feasibility of CO_2 injection and storage in deep aquifers. Uncoupled batch geochemical modeling and flow simulation are inadequate to describe the complex subsurface physical and chemical interactions expected to occur. A systematic process-based understanding of the coupled physical and chemical phenomena should be addressed. Here a coupled reactive geochemical transport model TOUGHREACT has been used to analyze aquifer CO_2 disposal in a refined

sediment of the Gulf Coast. The mineralogy used in the simulations is similar to that commonly encountered in sedimentary basins. A number of simulations were performed for analyzing the sensitivity to kinetics of mineral dissolution and precipitation.

Deep subsurface environments are typically strongly reducing. Introduction of CO_2 into an otherwise reducing environment will set up chemical potential gradients that may be favorable for bacterial activity. Microbial organisms may be able to utilize CO_2 to generate energy, and also use it as a source of carbon. At this time no empirical information on the potential role of microbes in aquifer disposal of CO_2 is available, and no microbial activity has been included in our models.

We first give a brief description of the multiphase fluid flow and geochemical transport computer model TOUGHREACT. Then we present the problem setup including conditions and parameters of fluid flow and geochemistry used for the deep aquifer system. Next we report modeling results including changes in mineral abundance, CO2 sequestration capability by secondary carbonate precipitation, and porosity and permeability change. Finally, we present discussion and conclusions from the reactive geochemical modeling analysis for CO_2 disposal in deep aquifers.

2. Simulation approach

2.1. Flow and chemistry

Xu and Pruess (1998) developed a non-isothermal reactive geochemical transport model, TOUGHREACT, by introducing reactive geochemistry into the framework of the existing multi-phase fluid and heat flow code TOUGH2 (Pruess, 1991; Pruess et al. 1999). For simulating fluid flow induced by CO_2 injection into deep aquifers, Pruess and Garcia (2001) developed a fluid property module ECO2 for TOUGH2. ECO2 provides an accurate description of the thermophysical properties of mixtures of water and CO_2 at conditions that may typically be encountered in brine formations of interest for CO_2 disposal ($T > 35\ ^oC$; $75\ bars \leq P \leq 400\ bars$). For analyzing reactive fluid and chemical interaction with rock minerals induced by CO_2 disposal, we combined the reactive geochemistry part of the TOUGHREACT code with TOUGH2/ECO2, resulting in a new improved reactive geochemical transport simulator TOUGHREACT/ECO2.

2.2. Simulation method

Our modeling of flow and transport in geologic media is based on space discretization by means of integral finite differences (Narasimhan and Witherspoon, 1976). An implicit time-weighting scheme is used for the individual components of the model: flow, transport, and geochemical reactions. TOUGHREACT/ECO2 uses a sequential iteration approach similar to Yeh and Tripathi (1991), and Walter et al (1994). After solution of the flow equations, the fluid velocities and phase saturations are used

for chemical transport simulation. The chemical transport is solved on a component basis. The resulting concentrations obtained from the transport are substituted into the chemical reaction model. The system of chemical reaction equations is solved on a grid-block basis by Newton-Raphson iteration, similar to Parkhurst (1980), Reed (1982), and Wolery (1992). The chemical transport and reactions are iteratively solved until convergence. Full details on numerical methods are given in Xu and Pruess (1998, 2001).

2.3. Process capabilities

The simulator can be applied to one-, two-, or three-dimensional porous and fractured media with physical and chemical heterogeneity, and can accommodate any number of chemical species present in liquid, gas and solid phases. A wide range of subsurface thermo-physical-chemical processes is considered. The major processes considered for fluid and heat flow are: (1) fluid flow in both liquid and gas phases under pressure and gravity forces, (2) capillary pressure effects for the liquid phase, and (3) heat flow by conduction, convection and diffusion. Transport of aqueous and gaseous species by advection and molecular diffusion is considered in both liquid and gas phases. Aqueous chemical complexation and gas (CO_2) dissolution and exsolution are considered under the local equilibrium assumption. Mineral dissolution and precipitation can be modeled subject to either local equilibrium or kinetic conditions. Dissolution and precipitation of all minerals in simulations presented in this paper are modeled under kinetic conditions. The kinetic rate law used is given in Appendix A. The activity of aqueous species is equal to the product of the activity coefficient and molar concentration. Aqueous species activity coefficients with the exception of CO_2(aq) are

calculated from the extended Debye-Hückel equation (Helgeson and Kirkham, 1974). CO_2(aq) activity coefficient and CO_2(g) fugacity coefficient are functions of pressure, temperature and salinity (details on calculations are presented in Appendix C of Xu et al. (2001). Activities of pure mineral phases and H_2O are assumed to be one. The oxygen approach is used for formulating redox reactions, which is based on attributing the oxidizing potential to the dissolved oxygen (Nordstrom and Muñoz, 1986; Wolery, 1992).

2.4. Porosity and permeability change

Temporal changes in porosity and permeability due to mineral dissolution and precipitation can modify fluid flow. This feedback between transport and chemistry can be important and can be considered in our model, but a rather large computational penalty has to be paid if this is modeled explicitly. Alternatively, the model can monitor changes in porosity and permeability during the simulation from changes in mineral volume fractions without feedback to the fluid flow. Changes in porosity during the simulation are calculated from changes in mineral volume fractions. A simple Kozeny-Carman grain model based on spheres was used to calculate changes in permeability due to changes in porosity (Bolton et al., 1999). The Kozeny-Carman equation relates the permeability k (in m^2) to the porosity (ϕ) by

$$k = \frac{R_0^2}{45}\left(\frac{\phi^3}{(1-\phi)^2}\right) \quad (1)$$

where R_0 is the initial local spherical close pack radius. Based on Eq. (1), the ratio of the permeability k to initial permeability k_0 can be expressed as

$$\frac{k}{k_0} = \left(\frac{\phi}{\phi_0}\right)^3 \left(\frac{1-\phi_0}{1-\phi}\right)^2 \tag{2}$$

where ϕ_0 is the initial porosity. The porosity-permeability correlation in geologic media depends on a complex interplay of many factors, such as pore size distribution, pore shapes, and connectivity (Verma and Pruess, 1988). Additional porosity-permeability relationships will be considered in the future.

3. Definition of Test Problem

The response of deep saline aquifers to CO_2 injection will depend on many factors, including formation permeability and porosity, presence of heterogeneities such as faults and layers of high or low permeability, physical and chemical characteristics of the brines, and nature of the mineral phases that are present. A great deal of specific and detailed information will be required to assess the feasibility of disposing of CO_2 in a brine formation at a particular site, and to develop engineering designs for CO_2 disposal systems. Before moving into site-specific investigations, it is necessary to explore features and issues related to aquifer disposal of CO_2 in a generic manner. This can be done by investigating models of deep brine systems that abstract from site-specific particulars and instead attempt to represent features that may be common to many such systems.

A basic issue in aquifer disposal of CO_2 is the physical and chemical behavior in the vicinity of a CO_2 injection well. Previous numerical studies have investigated simple models of one-dimensional and two-dimensional radial flow to examine the displacement of formation waters by injected CO_2 (Pruess et al., 2001; Pruess and Garcia, 2001). These studies have provided initial insight into issues of volumetric sweep, CO_2 storage capacity, and pressurization effects that would arise from large-scale CO_2 injection. Exploratory studies of geochemical effects have also been conducted, using a zero-dimensional batch reaction approach to model the chemical reactions that would take place when different mineral assemblages are exposed to CO_2 at high pressures in the presence of brine (Perkins and Gunter, 1996; Gunter et al., 1997; Xu et al., 2001). The

present study combines the simple 1-D radial model previously investigated by Pruess et al. (2001) with the batch chemical reaction model of Xu et al. (2001), in a first attempt to model the processes of fluid flow and chemical reactions near a CO_2 injection well in a coupled manner.

3.1 Saline aquifer

The aquifer is assumed to be infinite-acting and homogeneous with a thickness of 100 m, containing a 1 M NaCl brine at a constant temperature of 40 ^{o}C. A 1-D radial model is used. This simplification does not consider non-uniform sweep that may occur due to formation heterogeneities, or due to buoyancy forces that would tend to drive CO_2 towards the top of the aquifer. In future studies we plan to examine such multidimensional flow effects. Some justification for a 1-D approach can be derived from the slow rates and long time scales of geochemical changes, which will allow processes to be played out that over time will make the distribution of CO_2 more uniform. Initially, injected CO_2 will tend to accumulate and spread out near the top of permeable intervals, partially dissolving in the aqueous phase. CO_2 dissolution causes aqueous-phase density to increase by a few percent. This will give rise to buoyant convection where waters enriched in CO_2 will tend to migrate downward (Weir et al., 1995; Garcia, 2002). The process of CO_2 dissolution and subsequent aqueous phase convection will tend to mix aqueous CO_2 in the vertical direction. The time scale for significant convective mixing is likely to be slow (of the order of tens to hundreds of years; J. Ennis-King, private communication, 2001), and may be roughly comparable to time scales for significant geochemical interactions of CO_2.

The well field is modeled as a circular region of 8,000 m radius into which CO_2 is injected uniformly at a constant total rate of 100 kg/s (≈ 8,640 tonnes per day), For this injection rate, the amount of CO_2 injected is approximately equal to the generation of a 286 MW coal-fired power plant (Hitchon, 1996). A 1-D radial grid was used with a spacing gradually increasing away from the well. Parameter specifications were chosen representative of conditions that may be encountered in brine aquifers at a depth of order 1 km (Table 1). The CO_2 injection was assumed to occur over a period of 100 years. The fluid flow and geochemical transport simulation was run for a period of 10,000 years.

Table 1. Hydrogeologic parameters for the radial fluid flow problem.

Aquifer thickness Permeability Porosity Compressibility Temperature Pressure CO_2 injection rate	100 m 10^{-13} m^2 0.10 $1x10^{-8}$ Pa^{-1} 40 ^0C 100 bar 100 kg/s
Relative permeability	
Liquid (van Genuchten, 1980): $k_{rl} = \sqrt{S^*}\left\{1-\left(1-\left[S^*\right]^{1/m}\right)^m\right\}^2$ irreducible water saturation exponent	$S^* = (S_l - S_{lr})/(1-S_{lr})$ $S_{lr} = 0.00$ $m = 0.457$
Gas (Corey, 1954):	
$k_{rg} = (1-\widehat{S})^2(1-\widehat{S}^2)$ irreducible gas saturation	$\widehat{S} = \dfrac{(S_l - S_{lr})}{(S_l - S_{lr} - S_{gr})}$ $S_{gr} = 0.05$
Capillary pressure	
van Genuchten (1980) $P_{cap} = -P_0\left(\left[S^*\right]^{-1/m} - 1\right)^{1-m}$ irreducible water saturation exponent strength coefficient	$S^* = (S_l - S_{lr})/(1-S_{lr})$ $S_{lr} = 0.00$ $m = 0.457$ $P_0 = 19.61\,kPa$

3.2 . Geochemical system

A proxy for a sediment from the United States Gulf Coast based on Apps (1996) was used for the present reactive geochemical transport simulations. This mineralogy is similar to that commonly encountered in sedimentary basins. Apps (1996) presented a batch geochemical simulation of the evolution of Gulf Coast sediments as a basis for interpreting the chemical processes relating to the deep injection disposal of hazardous and industrial wastes. Gulf Coast Mesozoic and Tertiary sediments are characterized by rapid burial and incorporation of significant amounts of organic matter. Maturation of the organic matter into petroleum and natural gas, and its migration into numerous structural traps is a characteristic of these sediments. Therefore, a simulation should incorporate a representation of maturing organic matter. Another feature of relevance is the entrapment of evaporite salt beds during sedimentary accumulation. Over time, the salt has migrated into diapirs, modifying sedimentary accumulation during concurrent sedimentation and subsidence, and generating salt domes, which commonly trap oil and gas accumulations along their flanks. The salt domes are known to dissolve partially into groundwaters, elevating the salinity. Thus a simulation should also include an initial concentration of dissolved sodium chloride.

The initial mineral abundances used in the present reactive geochemical transport modeling (Table 2), are refined from the previous batch geochemical modeling study by Xu et al. (2001). The need to refine the mineralogy arises because the nature of one-dimensional simulations involving reactive transport between multiple cellular systems differs significantly from earlier “black box” reaction progress simulations. In the latter

case, the chemical evolution of the system is insensitive to quasi-inert diluents such as quartz, and the emphasis is on computational efficiency and ensuring relatively accurate specification of the fractions of reactive mineral constituents. Hence, the proportion of quartz included in earlier simulations was adjusted to values substantially less than would be characteristic of a typical Gulf Coast saline aquifer. However, in the case of reactive chemical transport in systems involving a multiplicity of cells, changes in porosity due to the formation of secondary minerals, can have a pronounced effect on permeability and hence on the hydrodynamic characteristic of the system. It is therefore much more important that mineral fractions are representative.

The specification of aquifer mineralogy is determined in part by the availability of data. Most studies of Tertiary Gulf Coast sediments are concentrated in the state of Texas. The principal reservoir-quality sandstones within that region are respectively, the Frio, the Vicksberg and the Wilcox formations, all of which are found within the lower Tertiary. Of the three formations, the Frio was chosen as a representative candidate for the sequestration of supercritical carbon dioxide. It is the shallowest of the three formations, but located over much of its areal extent at depths between 5,000 and 20,000 ft, depths sufficient to ensure adequate CO_2 densities for effective storage.

Loucks et al. (1984) used the sandstone classification of Folk (1968) to describe sandstone reservoirs in the Lower Tertiary Gulf Coast sediments of Texas. This classification projects the composition of sandstones onto a ternary diagram in terms of the components: quartz, feldspar and rock fragments. According to these authors, the Frio shows the greatest variation in mineral composition ranging from poorly sorted fine-grained feldspathic litharenites to lithic arkoses to fine-grained lithic arkoses and sub-

arkoses (see Figure 1). For the purposes of this study, the approximate mean composition of the Frio in the Middle Texas region of the Gulf Coast was chosen. This composition is representative of a quartzose lithic arkose with 56% quartz (by weight), 28% feldspar and 16% lithic fragments. According to Loucks et al. (1984), the lithic fragments in the Frio formation of this region are predominantly volcanic fragments, although significant percentages of metamorphic rocks are present. Carbonate rock fragments are also present, but are less common than along the lower Texas Gulf Coast. The volcanic rocks of the lower Texas Gulf Coast are dominantly rhyolites and trachytes, which have been silicified or altered to chlorite. Those volcanic rocks of the middle Texas Gulf Coast are apparently of similar composition and provenance, but less abundant. The carbonate fragments were apparently locally derived from adjacent landmass caliche soils. Neither the provenance nor the character of the metamorphic rocks is described.

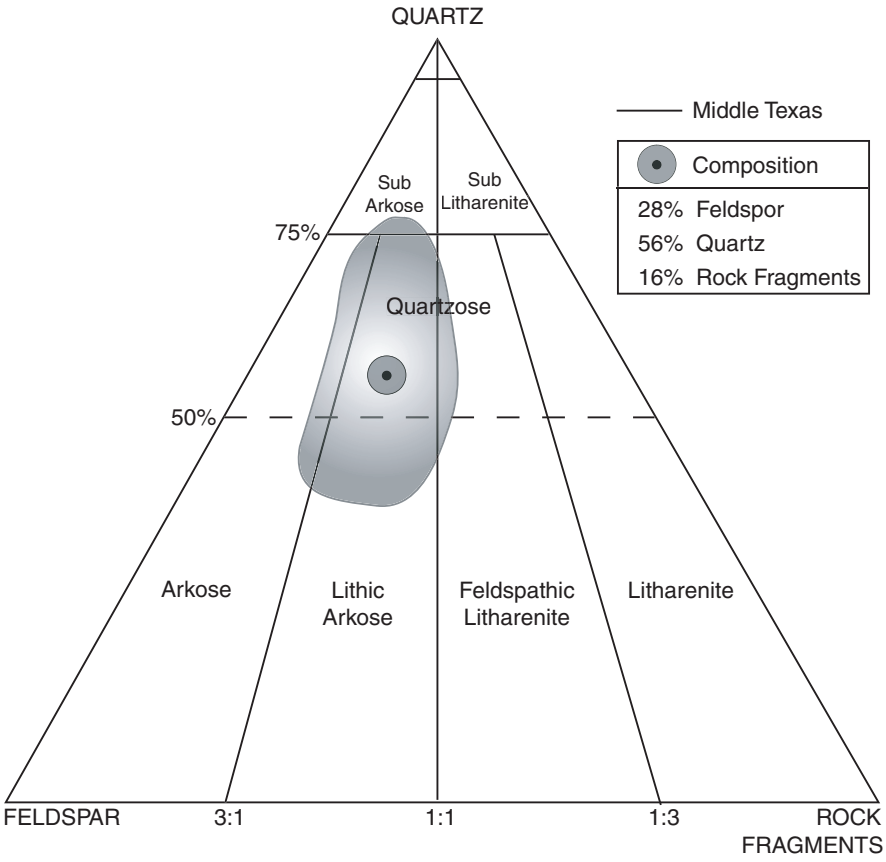

Figure 1. Selected mean composition of the Lower Tertiary Frio Formation of the middle Texas region of the Lower Tertiary Gulf Coast sediments (based on an analysis by Loucks et al. (1984) and classification by Folk (1968)).

For the purposes of simulation, the actual mineral composition of the sandstone is required. This necessitates knowing the fractions of plagioclases and alkali feldspars making up the feldspar component, and the mineralogy of the lithic fragments. Land (1984) reports that 1,634 electron probe point counts on 29 Frio formation rocks indicate that about 30 wt.% of the original feldspar was K-feldspar and the remainder was plagioclase having an average anorthite content of 20 wt.%. The concentration of potash feldspar is therefore somewhat higher than specified by Tempel and Harrison (2000) for the underlying Wilcox Formation who modeled a feldspathic litharenite comprising 25.8 wt.% plagioclase with content of 25 wt.% anorthite and 5 wt.% K-feldspar. The

composition of the lithic fragments has been described only in a qualitative sense, and therefore, the actual mineral composition can only be surmised. Furthermore, secondary minerals (calcite, clay minerals, and iron oxides) are not included in published lithological classifications. Therefore, the inclusion of these phases must also necessarily be determined subjectively.

The representative mineral composition of a quartzose lithic arkose from the Middle Texas area of the Frio formation given in Table 2 was assigned abundances using the following arguments:

- Two weight percent of calcite was added to reflect the presence of lithic fragments of caliche present in the Frio (Loucks et al., 1984).
- The observed presence of chlorite in lithic fragments of volcanic rock (Loucks et al., 1984) is represented by 3 wt.% clinochlore and 2 wt.% daphnite, representing the magnesium and ferrous end members, respectively of a chlorite solid solution. (TOUGHREACT does not presently have the capability of incorporating solid solutions.)
- A small amount of hematite (1 wt.%) was added to take into account the presence of ferric iron staining. The chosen concentration is consistent with independent modeling by Tempel and Harrison (2000).
- Organic Matter, as CH_2O, is arbitrarily assigned an abundance of 1 wt.%. The shale confining beds of the Gulf Coast, representing a substantially larger mass than the enclosed aquifers, are estimated to contain about 1 wt.% organic carbon, (Hunt, 1972, as cited by Franks and Forester (1984)). However, this abundance is probably much higher than is found in the sandstone matrix of contiguous aquifers. Given the fact that

the adjacent shales are probably the source of many of the secondary minerals in the aquifers, and that certain compromises have to be made in order to proceed with preliminary model approximations, it is reasonable to assume that the aquifers contain about 1 wt.% CH_2O as a first approximation.

- The concentrations of clay minerals, smectite, illite and kaolinite were arbitrarily assigned abundance of 4, 1 and 2 wt.% respectively and assigned as the residue of the mineral contribution by lithic fragments. The compositions of smectite and illite are those representative of illite/smectite (I/S) clays, typical of Gulf Coast sediments. The smectite could be of detrital or diagenetic origin, and could be separated from the lithic fragments, or included as an alteration product within the fragments.

Table 2. List of initial mineral volume fractions, possible secondary mineral phases, and their kinetic properties used in the simulation. All rate constants are listed for dissolution. (k_{25} is the kinetic constant at 25 ^{o}C, and E_a activation energy).

Mineral	Chemical composition	Wt. %	Vol.%	k_{25} (moles $m^{-2}s^{-1}$)	E_a (KJ/mol)	Reference
***Primary*:**						
quartz	SiO_2	56	49.7466	$1.2589x10^{-14}$	87.50	Tester et al. (1994)
kaolinite	$Al_2Si_2O_5(OH)_4$	2	1.8135	$1.00x10^{-13}$	62.76	Nagy (1995)
calcite	$CaCO_3$	2	1.7361	$1.60x10^{-9}$	41.87	Svensson and Dreybrodt (1992)
illite	$K_{0.6}Mg_{0.25}Al_{1.8}(Al_{0.5}Si_{3.5}O_{10})(OH)_2$	1	0.8586	$1.00x10^{-14}$	58.62	Knauss and Wolery (1989)
organic	CH_2O	1	2.6136	$1.00x10^{-13}$	0.0	assigned based on kaolinite
oligoclase	$CaNa_4Al_6Si_{14}O_{40}$	20	17.8155	$1.00x10^{-13}$	62.76	set to kaolinite
K-feldspar	$KAlSi_3O_8$	8	7.3611	$1.00x10^{-12}$	67.83	Blum and Stillings (1995)
smectite-Ca	$Ca_{0.145}Mg_{0.26}Al_{1.77}Si_{3.97}O_{10}(OH)_2$	4	3.5073	$1.00x10^{-14}$	58.62	set to illite
clinochlore	$Mg_5Al_2Si_3O_{10}(OH)_8$	3	2.6793	$1.00x10^{-13}$	62.76	set to Kaolinite
daphnite	$Fe_5Al_2Si_3O_{10}(OH)_8$	2	1.4211	$1.00x10^{-13}$	62.76	set to kaolinite
hematite	Fe_3O_3	1	0.4473	$1.00x10^{-13}$	0.0	Ague and Brimhall (1989)
porosity	------		10			
total	------		100			
***Secondary*:**						
albite-low	$NaAlSi_3O_8$		0.0	$1.00x10^{-12}$	67.83	Blum and Stillings (1995)
dolomite	$CaMg(CO_3)_2$		0.0	$0.60x10^{-9}$	41.8	assigned based on calcite
siderite	$FeCO_3$		0.0	$0.60x10^{-9}$	41.8	assigned based on calcite
smectite-Na	$Na_{0.290}Mg_{0.26}Al_{1.77}Si_{3.97}O_{10}(OH)_2$		0.0	$1.00x10^{-14}$	67.83	set to illite
pyrite	FeS_2		0.0	$1.00x10^{-13}$	0.0	Ague and Brimhall (1989)
graphite	C		0.0	$1.00x10^{-13}$	0.0	set to organic
dawsonite	$NaAlCO_3(OH)_2$		0.0	$1.00x10^{-12}$	67.83	set to k-feldspar

Dissolution of primary minerals proceeds under kinetic conditions. The rate law used is given in Eq. A.1 (in Appendix A) using two exponential parameters μ and n set equal to one (i.e., first order kinetics). Rate constants at any given temperature are calculated from Eq. A.2, using the kinetic constant at 25 ^{o}C (k_{25}) and activation energy (E_a). These kinetic parameters are also given in Table 2. Some kinetic parameters were taken directly from the published scientific literature. The references are listed in the last column of Table 2. Others were set to or modified from minerals with known kinetic properties. Precipitation of possible secondary minerals (Table 2 with an initial mineral volume fraction of zero) is represented using the same kinetic rate expression as that for dissolution. However, precipitation can differ in several respects, as nucleation, Ostwald ripening, crystal growth processes, and reactive surface areas must be taken into account in some circumstances (Plummer et al., 1978; Steefel and van Capellen, 1990). To simplify the description of precipitation kinetics, the precipitation kinetic constant for a secondary mineral is assumed to be one order of magnitude greater than its corresponding dissolution rate constant. Note that all rate constants in Table 2 (including secondary phases) are for dissolution. Because the rate constants assumed for precipitation reactions are larger than those for dissolution, formation of secondary minerals occurs effectively at conditions close to local equilibrium. A total specific surface area of 6,500 m^2/m^3 medium was used. The initial surface area of each primary mineral (Table 2) is calculated from its volume fraction multiplied by the total surface area. With time, the surface areas change in complex ways. In this study, however, we simply relate the surface areas of the primary minerals at some time to the mineral volume fraction by

$$A = A^0 \frac{V_f}{V_f^0} \tag{3}$$

where A, and V_f are the reactive surface area and volume fraction of a primary mineral, respectively, and superscript zero indicates the values at time t = 0. The reactive surface areas for secondary minerals are set to 650 m^2/m^3 at all times. Surface areas for clay minerals (illite, kaolinite, smectite-Na, and smectite-Ca) are increased by one order of magnitude.

The maturation of organic matter eventually leads to the formation of a carbon-rich residue such as vitrinite or asphaltene. In this study, we represent this residue as graphite, which we assume precipitates as a result of the dissolution of organic matter. Hence, its kinetic properties are assigned the same values as those of the proxy for organic matter.

Most solubility products for minerals were taken from the EQ3/6 V7.2b database (Wolery, 1992) that were derived from thermodynamic data using SUPCRT92 (Johnson et al., 1992), except for oligoclase, and organic matter that were calculated in the CO_2 disposal study (Xu et al., 2001).

Prior to CO_2 injection, a simulation of water-rock interaction was performed to obtain a nearly equilibrated water chemistry (see Table 3) using a pure 1.0 M solution of sodium chloride reacting with the primary minerals listed in Table 2 at a temperature of 40 ^oC. The resulting water chemistry was used for the initial condition of reactive geochemical transport simulations under CO_2 injection.

Table 3. Initial water chemical composition used for reactive geochemical transport simulations under CO_2 injection.

Chemical component	Concentrations (mol/kg H_2O)
Ca^{2+}	$3.470x10^{-3}$
Mg^{2+}	$1.637x10^{-4}$
Na^{+}	1.047
K^{+}	$1.801x10^{-2}$
Fe^{2+}	$4.469x10^{-7}$
$SiO_2(aq)$	$1.147x10^{-4}$
HCO_3^{-}	$9.291x10^{-4}$
SO_4^{2-}	$1.323x10^{-9}$
AlO_2^{2-}	$7.158x10^{-8}$
Cl^{-}	1.061
pH	7.7
Log(fo2(aq))	-69.312
T	40 ^{o}C

3.3. Parameter uncertainties

Estimated mineral dissolution rates cover a wide range of values. The documented values are cited under laboratory conditions of controlled pH and temperature, and fine grain size. Field effective values may be much lower than those reported from laboratory experiments (Nordstrom and Alpers, 1997). The evolution of surface area in natural geologic media is very complex, especially for multi-mineralic systems, and has not yet been quantitatively described. A reactive surface area, calculated from grain size, is often a poor estimate of the hydrologically accessible mineral surface area. The specific reactive surface areas may vary over several orders of magnitude depending on grain size, mineralogy, surface roughness, coatings, weathering, and biological effects (White and Peterson, 1990). We performed a number of simulations using different kinetic rate constants for mineral dissolution and precipitation. The rate constant sensitivity includes

the uncertainty arising from reactive surface area and rock mineral volume fraction, because the effective reaction rate is the product of kinetic rate constant and reactive surface area (See Equation A.1 in Appendix A). A sensitivity analysis could give some general understanding of its impact on the overall geochemical behavior of the system.

The first reactive geochemical transport simulation used the kinetic rate constants as given in Table 2. We refer to this simulation as base-case simulation. Previous study (Xu et al., 2001) shows that scaling kinetic rates by the same constant factor is equivalent to scaling the time coordinate and does not lead to different results. An increase in the rate is equivalent to a corresponding decrease in time scale. In this study, we examine the effect of changing mineral kinetic rates relative to one another based on the base-case simulation. The kinetic rate sensitivity simulations were performed by changing the kinetic rate constant of any mineral by one order of magnitude increase or decrease from the values given in Table 2.

4. Results and Discussion

4.1 Base-case

Figure 2 shows water saturations along the radial distance (gas CO_2 saturations are complementary to water saturations, or $S_g = 1- S_l$). Water saturations are lower close to the CO_2 injection well. In the first 11.5 m water is completely removed by CO_2 gas at 100 years (Figure 2b). Subsequently water gradually flows back because CO_2 injection has been stopped.

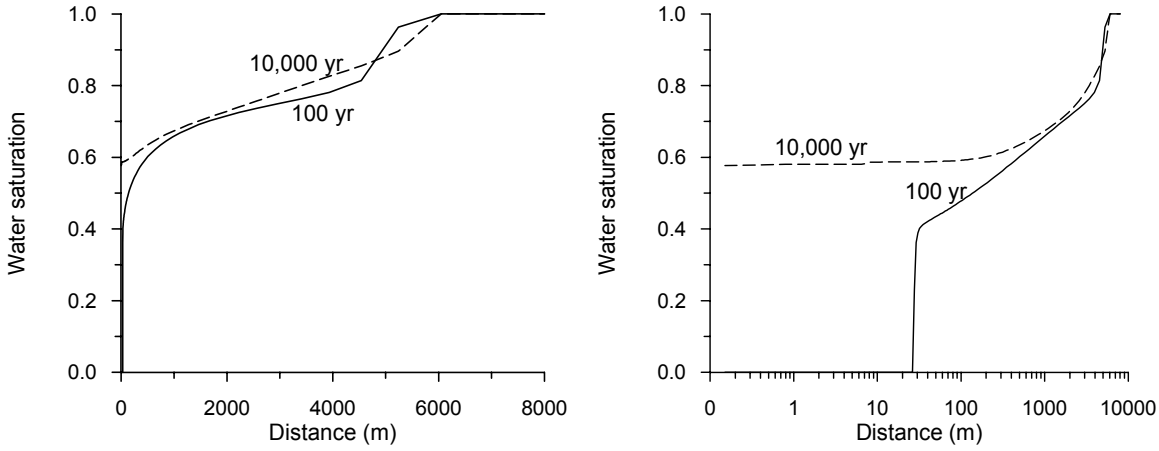

(a) Linear scale (b) Log10 scale

Figure 2. Water saturations at different times for the 1-D radial flow problem.

The pH and Eh are strongly buffered by CO_2 gas pressure. A pH of about 5 and an Eh of 0.28 V are obtained in the presence of high pressure CO_2. The low pH induces strong mineral alteration. Changes of mineral abundances after 10,000 years are presented in Figure 3. Mineral abundance is expressed as volume fraction of mineral in

terms of the bulk medium. Significant oligoclase dissolves after 10,000 years (Figure 3a). Note that the CO_2 plume extends outward to about 6,000 m, and this is the reason for the abrupt changes in mineral abundance seen in Figure 3 near 6,000 m. The dissolution peak occurs just behind the gas CO_2 front because water saturation is higher at this location and amounts of mineral dissolution and precipitation are proportional to the amount of water in the model. Some clinochlore and daphnite dissolution (Figure 3b) also occurs with a similar pattern (Figure 3b). Slight dissolution of hematite and organic matter (Figure 3b) also occurs. As some minerals dissolve, secondary phases are formed. Precipitation of calcite and siderite (Figure 3c) occurs due to oligoclase and daphnite dissolution and carbonate availability by the CO_2 injection. Significant dawsonite (Figure 3d) precipitates due to dissolution of alumino-silicate minerals. No dolomite precipitation is observed in this base-case simulation. Some of the CO_2 is immobilized by precipitation of the three carbonate minerals (calcite, siderite, and dawsonite). In addition to carbonates, significant precipitation of quartz, smectite-Na, and albite-low are seen from Figure 3d. Slight precipitation of k-feldspar and kaolinite (Figures 3a), and illite (Figure 3d) is observed. Organic matter dissolution generates a slight amount of graphite. Pyrite precipitation is not observed. The cumulative sequestration of CO_2 by secondary carbonates is presented in Figure 4. Figure 5 shows evolution of total CO_2 sequestered in the three phases for the entire reservoir. Significant CO_2 mineral trapping starts at 500 years and increases with time. After 10,000 years, CO_2 mineral trapping is comparable to CO_2 dissolution in pore waters. The solubility trapping increases very slightly with time due to slight movement of the CO_2 plume. Gas CO_2 is dominant over the simulation time, but it decreases with time. The addition of CO_2 mass as secondary carbonates to the solid

matrix causes a decrease in porosity (Figure 6), and in turn a decrease in permeability. A maximum porosity decrease of 3% and permeability decrease of 7 % can be observed. Finally, we present concentrations of total dissolved chemical components in Figure 7.

Because the present reactive geochemical transport simulation uses a refined mineral composition from the earlier batch geochemical simulation (Xu et al., 2001), the mineral alteration pattern and changes in abundance cannot directly be compared with the earlier results. In the present study, the addition of Mg-bearing and Fe-bearing minerals clinochlore ($Mg_5Al_2Si_3O_{10}(OH)_8$)) and daphnite ($Fe_5Al_2Si_3O_{10}(OH)_8$)) causes precipitation of carbonate minerals dolomite ($CaMg(CO_3)_2$) and siderite ($FeCO_3$). We also allow secondary carbonate dawsonite ($NaAlCO_3$ $(OH)_2$) to precipitate. However, both simulations obtain precipitation of carbonate mineral calcite, clay minerals, and decrease in porosity.

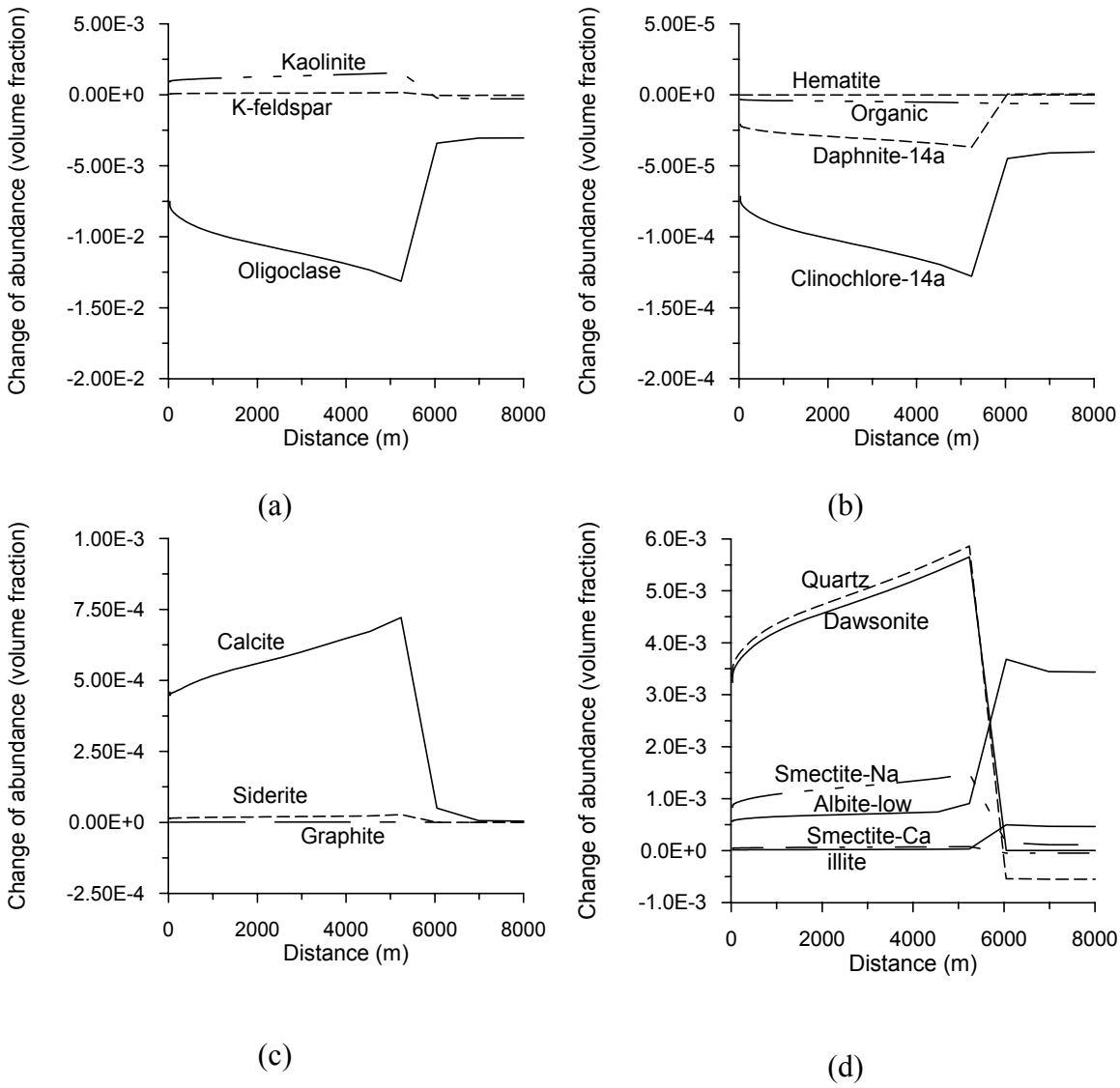

Figure 3. Change of mineral abundance (negative values indicate dissolution and positive precipitation) after 10,000 years for the 1-D radial flow problem. Note that scales for change of abundance are different among the four figures.

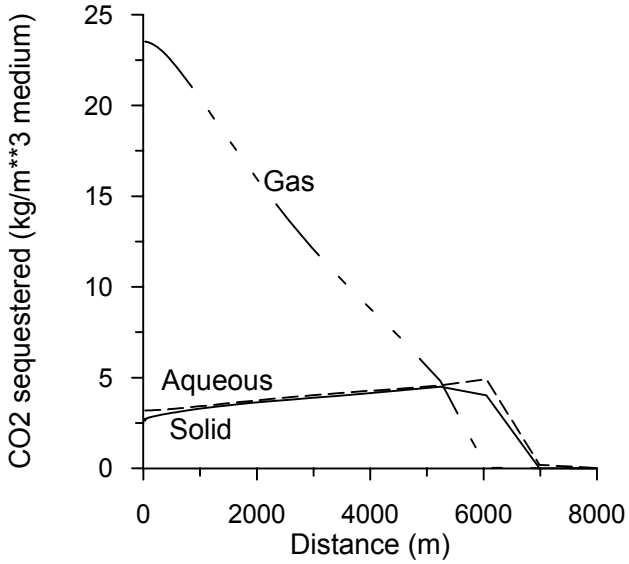

Figure 4. Cumulative CO_2 sequestration in different phases after 10,000 years.

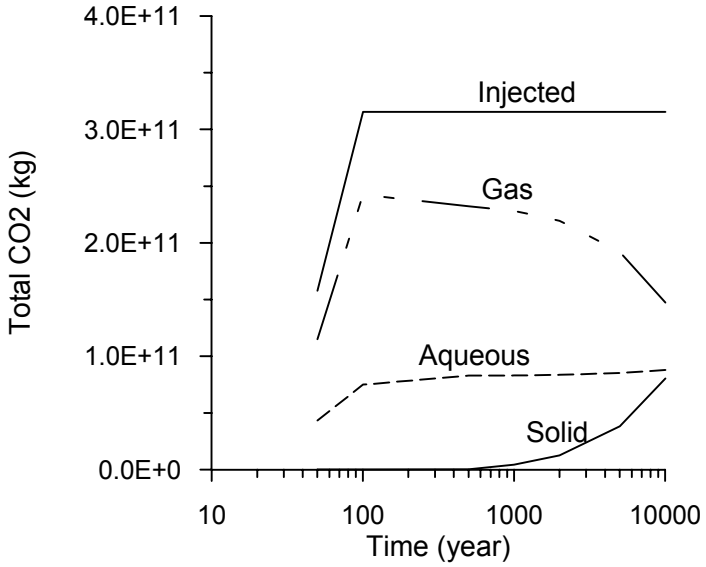

Figure 5. Total CO_2 sequestered in the three phases for the entire reservoir.

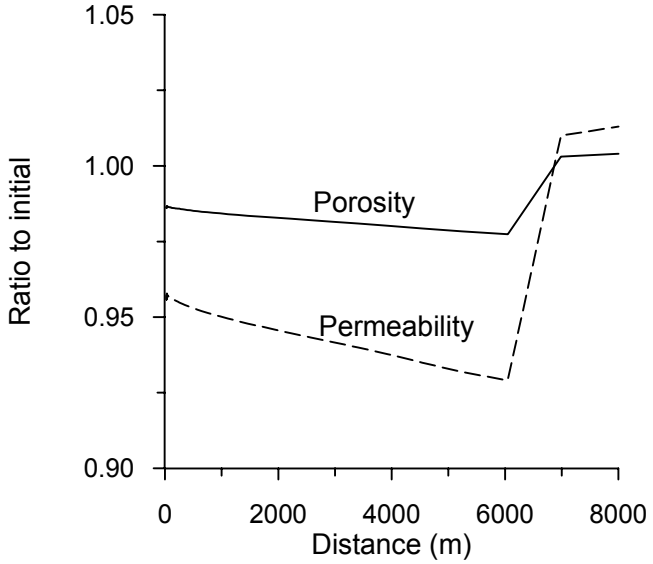

Figure 6. Ratio of porosity (ϕ/ϕ_0) and permeability (k/k_0) to initial time after 10,000 years.

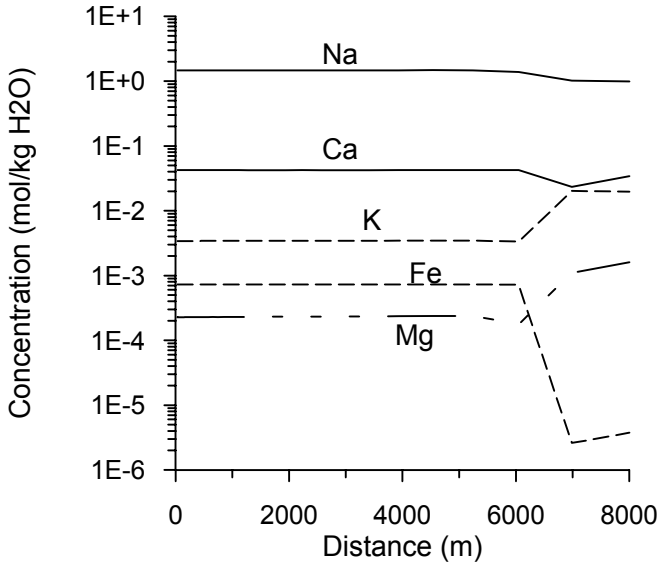

Figure 7. Concentrations of total dissolved chemical components after 10,000 years.

4.2. Sensitivity to reaction rate

Quartz

Figure 8 shows cumulative CO_2 sequestered by carbonate mineral precipitation (a) and porosity ratio (b) after 10,000 years obtained by an increase and a decrease of one order of magnitude of the quartz kinetic rate constant together with the results of base-case simulation. An increase in quartz kinetic rate enhances CO_2 sequestration (Figure 8a) and porosity reduction (Figure 8b). An increase in quartz kinetic rate causes more quartz precipitation. Consequently, significant dolomite precipitation (Figure 9a) occurs, which is not observed in the base-case simulation (Figure 3c). Calcite precipitation is slightly lower than that of base-case simulation (compare Figure 9a to 3c). More dawsonite precipitation occurs (compare Figure 9b to 3d). Less smectite-Ca and smectite-Na precipitation occurs (compare Figure 9b to 3d). Albite-low precipitation is not seen in this simulation because of more quartz precipitation. When the rate constant decreases one order of magnitude, the pattern of mineral dissolution and precipitation is similar to that of the base-case with a slight decease of CO_2 sequestration (Figure 8a).

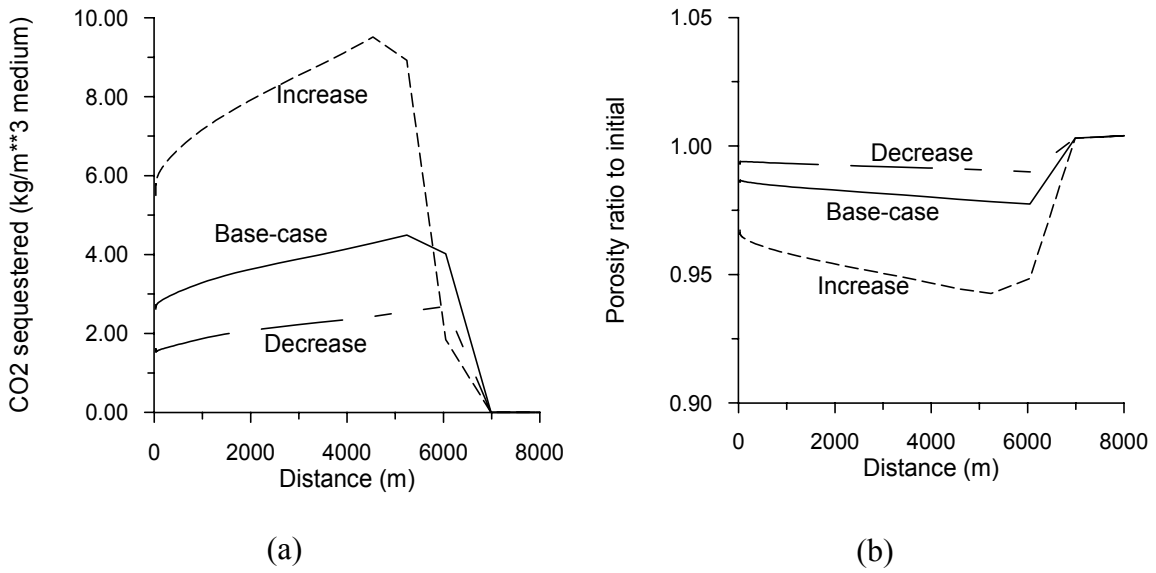

(a) (b)

Figure 8. Cumulative CO_2 sequestered by carbonate mineral precipitation (a) and porosity ratio (b) after 10,000 years for different quartz kinetic rate constants.

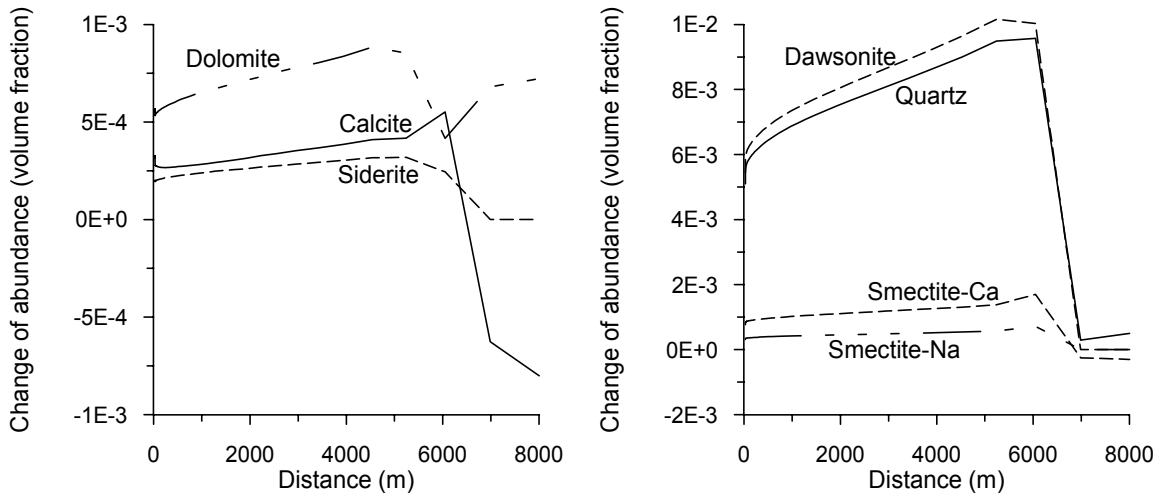

(a) (b)

Figure 9. Change of mineral abundance after 10,000 years obtained by an increase of one order of magnitude of quartz kinetic rate constant.

Oligoclase

When the oligoclase dissolution kinetic rate constant is increased by one order of magnitude, the pattern of mineral dissolution and precipitation is similar to that of the base-case. Mineral CO_2 sequestration increases slightly (Figure 10a) and porosity ratio decreases slightly (Figure 10b) from the base-case. A decrease in the oligoclase kinetic rate constant causes a significant decrease in CO_2 sequestration by secondary carbonate precipitation and less porosity reduction. Calcite dissolves (Figure 11a) rather than precipitates as in the base-case (Figure 4c). Dolomite precipitation occurs. Dawsonite precipitation is slightly lower than in the base-case (compare Figure 11b to 3d). A decrease in oligoclase dissolution rate results in less quartz and smectite precipitation (compare Figure 11b to 3d). Albite-low precipitation does not occur.

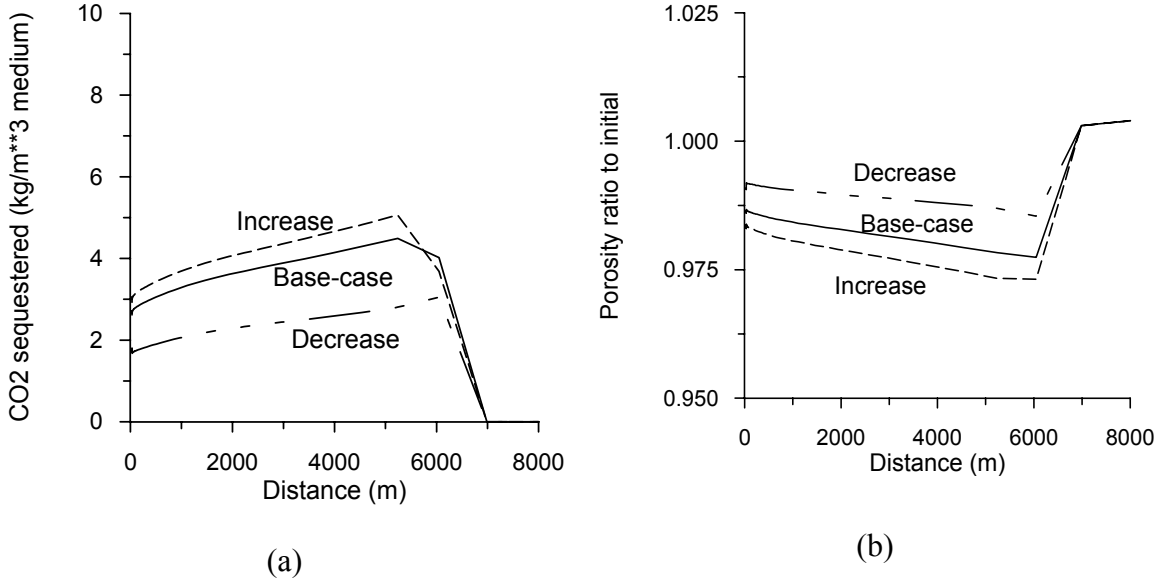

Figure 10. Cumulative CO_2 sequestered by carbonate mineral precipitation (a) and porosity ratio to initial time (b) after 10,000 years for different oligoclase kinetic rate constants.

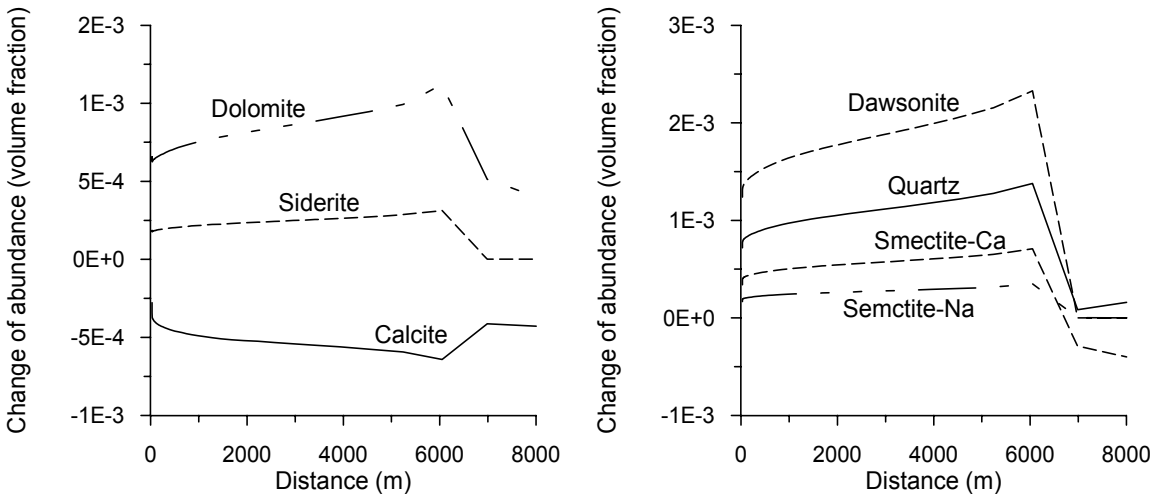

Figure 11. Change of mineral abundance after 10,000 years obtained by a decrease of one order of magnitude of oligoclase kinetic rate constant.

Clinochlore

Figure 12 shows cumulative CO_2 sequestered by carbonate mineral precipitation (a) and porosity ratio after 10,000 years obtained by an increase and a decrease of one order of magnitude of the clinochlore kinetic rate constant together with the results of base-case simulation. An increase in clinochlore kinetic rate significantly enhances CO_2 sequestration (Figure 12a) and porosity reduction (Figure 12b). The increase in dissolution of the Mg bearing mineral clinochlore ($Mg_5Al_2Si_3O_{10}(OH)_8$) results in a very significant dolomite ($CaMg(CO_3)_2$) precipitation (Figure 13a). Consequently calcite dissolves rather than precipitates as in the base-case. Slight siderite precipitation occurs. Dawsonite precipitation still occurs with similar amount (compare Figure 13b to 2d). When the rate constant decreases one order of magnitude, the pattern of mineral dissolution and precipitation is similar to that of the base-case with a slight decrease of CO_2 sequestration and porosity reduction (Figure 12).

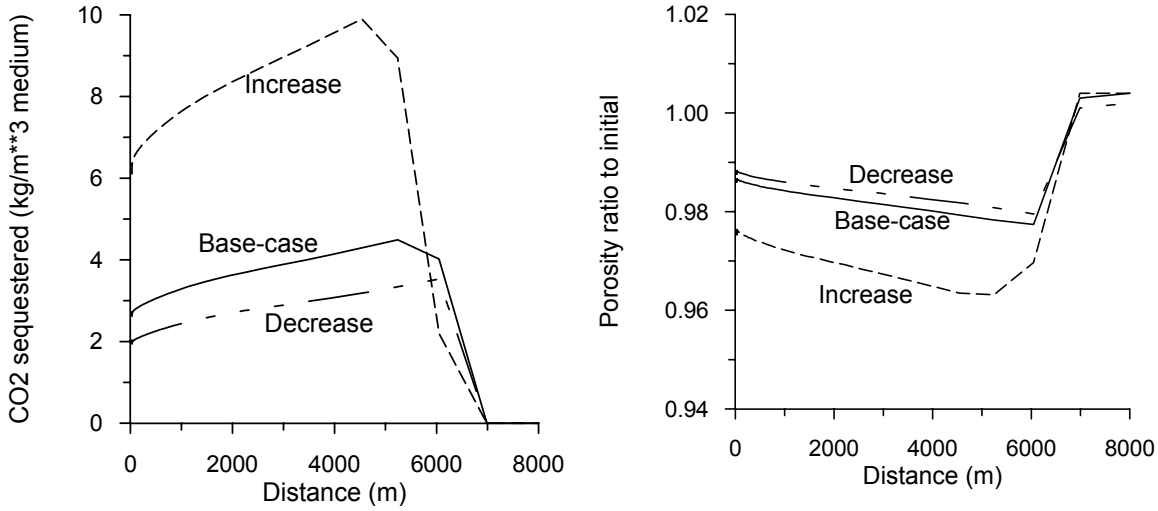

(a) (b)

Figure 12. Cumulative CO2 sequestered by carbonate mineral precipitation (a) and porosity ratio to initial time (b) after 10,000 years for different clinochlore kinetic rate constants.

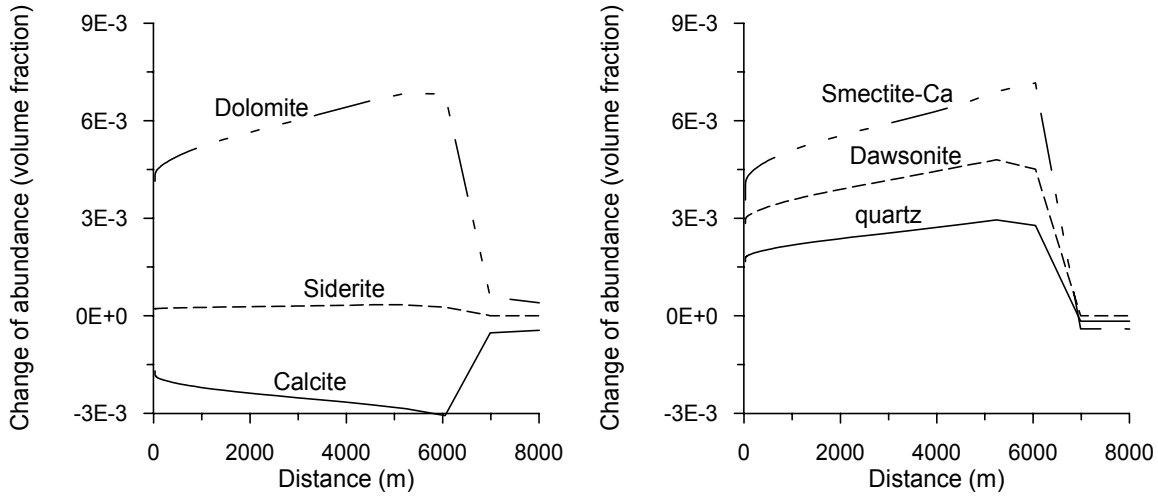

(a) (b)

Figure 13. Change of mineral abundance after 10,000 years obtained by an increase of one order of magnitude of clinochlore kinetic rate constant.

Daphnite

Figure 14 shows cumulative mineral CO_2 sequestration (a) and porosity ratio (b) after 10,000 years obtained by changes of one order of magnitude of the daphnite kinetic rate constant together with results of the base-case simulation. Note that the Fe-bearing mineral daphnite ($Fe_5Al_2Si_3O_{10}(OH)_8$) has a similar chemical composition as clinochlore ($Mg_5Al_2Si_3O_{10}(OH)_8$) except that Mg is replaced by Fe. An increase in the daphnite kinetic rate constant enhances CO_2 sequestration (Figure 14a) and porosity reduction (Figure 14b). It also results in significantly greater siderite ($FeCO_3$) precipitation (Figure 15a) than the base-case. In addition, slightly more calcite precipitation is observed. In this case, dolomite precipitation does not occur. Dawsonite precipitation is somewhat reduced (compare Figure 15b to 3d). The results obtained with a decrease in the rate constant are similar to those of the base case.

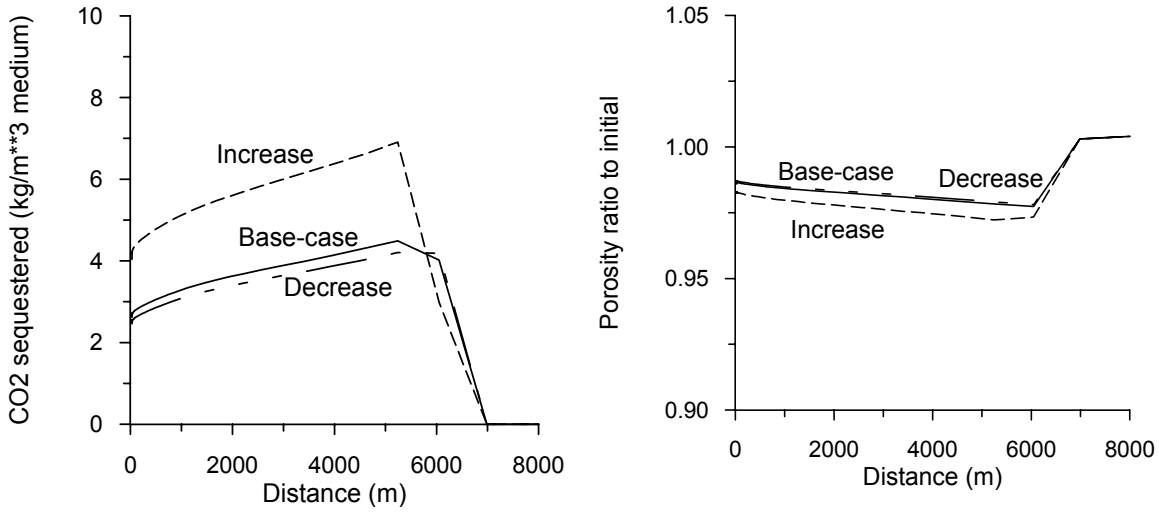

(a) (b)

Figure 14. Cumulative CO2 sequestered by carbonate mineral precipitation (a) and porosity ratio to initial time (b) after 10,000 years for different daphnite kinetic rate constants.

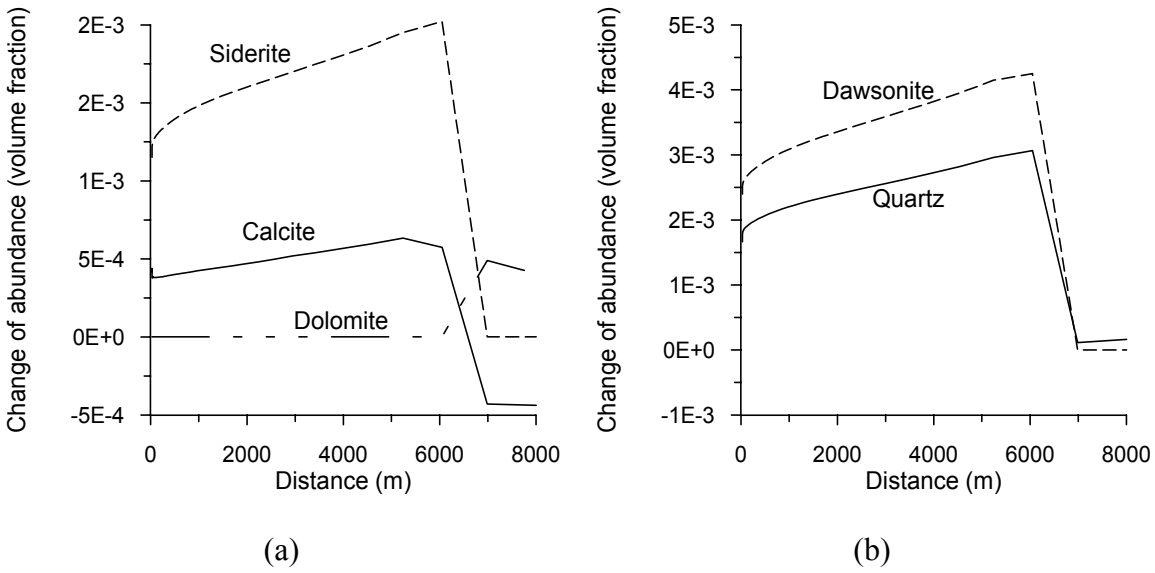

Figure 15. Change of mineral abundance after 10,000 years obtained by an increase of one order of magnitude of daphnite kinetic rate constant.

Other minerals

Changes of kinetic rate constants for other minerals do not result in significant changes in the pattern and magnitude of mineral dissolution and precipitation. The CO_2 sequestered by secondary carbonates and porosity reduction are similar to those of the base case. The precipitation of secondary minerals including calcite, illite, smectite-Ca, smectite-Na, albite-low dolomite, siderite, and dawsonite mainly depends on dissolution of primary minerals such as oligoclase, clinochlore, and daphnite. Amounts of k-feldspar and kaolinite dissolution are small, so changes in their rate constants have no significant impacts. Dissolution of organic matter and precipitation of graphite do not significantly affect the overall geochemical evolution. Hematite dissolution is very small and pyrite precipitation is not observed in any of the simulations.

4.3. Discussion

CO_2 sequestration by carbonate minerals

In our simulations, the secondary carbonate minerals calcite ($CaCO_3$), dolomite ($CaMg(CO_3)_2$), siderite ($FeCO_3$), and dawsonite ($NaAlCO_3(OH)_2$) are formed in the presence of high pressure CO_2. Variations in the precipitation of secondary carbonate minerals depend on rock mineral composition and the kinetic rate for dissolution. For the base-case simulation, dawsonite is the dominant CO_2 trapping mineral and no dolomite is formed. For the simulation using a decrease of one order of magnitude of the oligoclase dissolution rate constant, dolomite precipitates (Figure 11) and calcite dissolves rather than precipitates as in the base case. The simulation with an increase of clinochlore (Mg-bearing mineral, ($Mg_5Al_2Si_3O_{10}(OH)_8$)) dissolution rate results in dolomite as a dominant CO_2 trapping mineral and calcite dissolution (Figure 13). Similarly, an increase of daphnite (Fe-bearing mineral, ($Fe_5Al_2Si_3O_{10}(OH)_8$)) dissolution rate results in significant siderite precipitation. For most simulation cases, the CO_2 mineral-trapping capability after 10,000 years is comparable with that of solubility trapping (Figure 4, about 2 to 5 kg CO_2 per cubic meter medium). Under favorable conditions, such as an increase in the abundance or kinetic dissolution rate constant of the Mg-bearing mineral clinochlore, the capacity reaches a maximum value of 10 kg CO_2 per cubic meter medium (Figure 12a). The actual trapping capabilities also depend on many other factors such as porosity, rock mineral composition, gas pressure, and temperature of the deep aquifer system studied. For the time frame considered (10,000 years in present simulations), the largest CO_2 trapping mechanism is that of hydrodynamic trapping (Figure 4). Even though mineral

trapping is not the dominant mechanism, it is important because it provides amount of CO_2 trapped in minerals that is essentially permanent and increases with time.

For Gulf Coast sediments used in the simulations, all the above-mentioned CO_2 trapping minerals are formed in response to CO_2 injection, which may represent a favorable mineralogical condition. For example, the precipitation of siderite, either as a discrete carbonate or as a solid solution in more abundant Ca-Mg carbonates, or as ankerite ($(Mg,Ca,Fe(II))CO_3$), is conditioned by the redox state of the system.

Reaction kinetics

The time needed to sequester CO_2 in mineral phases is uncertain, because mineral kinetic properties and reactive surface areas are not well constrained. As previously noted by Xu et al. (2001), scaling surface areas by the same constant factor is equivalent to scaling the time coordinate and does not lead to significantly different results. An increase in the surface areas is equivalent to a decrease in time scale. In the present work, we have examined the effects of changing mineral kinetic rates relative to one another. The previous and the present sensitivity simulations cannot cover all combinations of changes in mineral kinetic rate. Simulations on other possible combinations will be addressed in the future. Alteration of the predominant host rock aluminosilicate minerals is very slow and is not experimentally accessible under ambient deep-aquifer conditions. Studies on rock alteration in natural CO_2 reservoirs may give some constraints on kinetic rates of mineral dissolution and precipitation.

The reaction time is a relative concept, and is affected by the fluid transport time scale. The reaction may be fast enough to form effective CO_2 mineral traps given a long

residence time of a packet of fluid in a deep aquifer. The difference between reaction and transport time scales may help ensure that CO_2 mineral trapping would be complete before any packet of fluid reaches the surface.

Changes in porosity

All simulations demonstrate that rock alteration after CO_2 injection results in decreased porosity (Figures 4, 8b, 10b, and 12b), because CO_2 mass is added to the solid matrix. A maximum 3% porosity decrease is obtained in our reactive geochemical simulations. A small decrease in porosity may result in a significant decrease in permeability.

5. Comparison with observations of natural diagenesis in Gulf Coast sediments

Some field observations concerning the natural diagenesis of Gulf Coast sediments are available. To compare with these observations, we present the simulated changes of mineral abundance in Figures 16 for distant region of the aquifer that are not affected by CO_2 injection. The comparison of mineral alteration for natural CO_2 reservoirs will be addressed in the future.

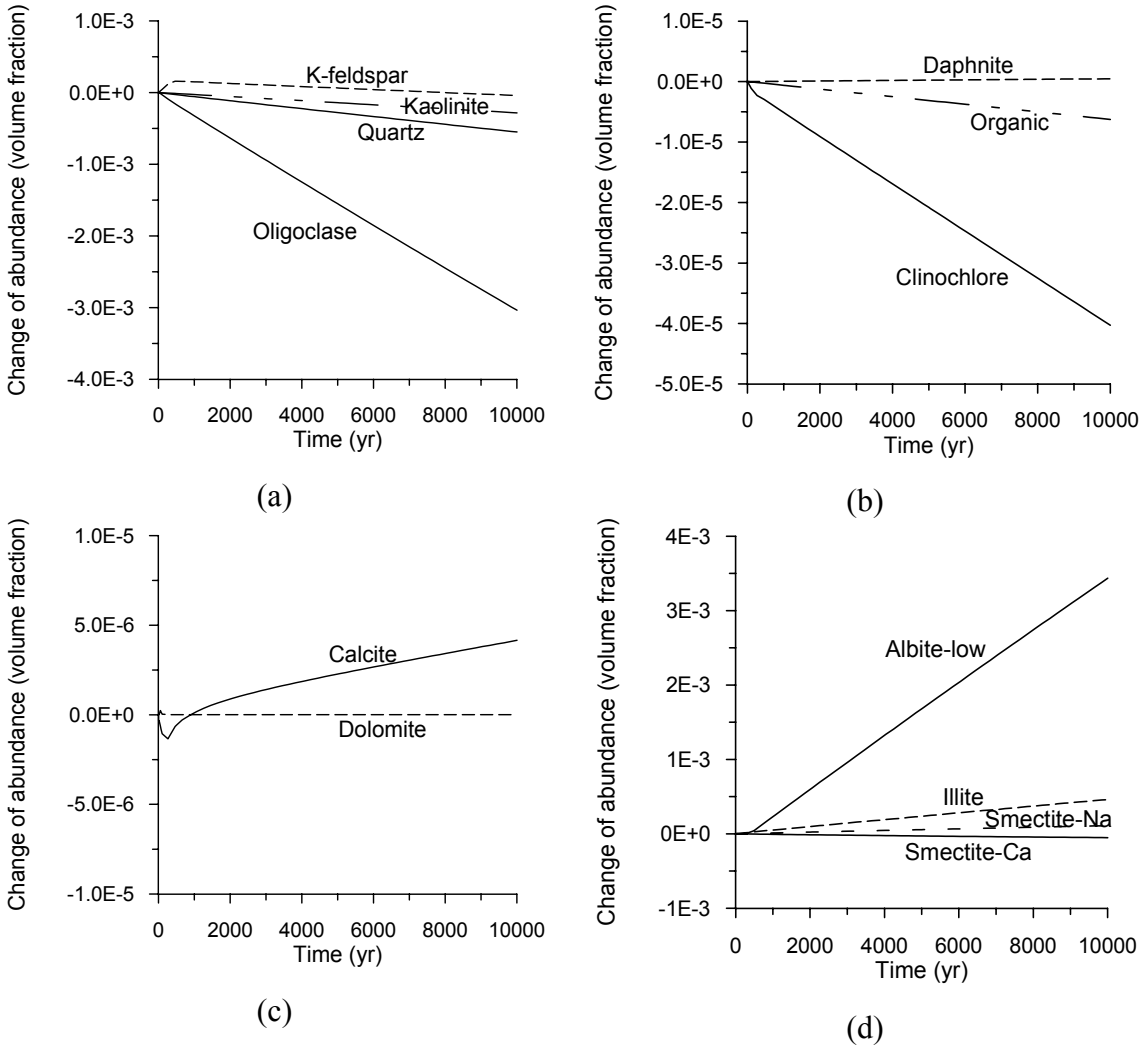

Figure 16. Change of mineral abundance vs. time in aquifer regions that not affected by CO_2 injection).

The current modeling makes many simplifications and also gives a limited account of the complexities of actual diagenesis in the field. Some of the processes and conditions not included in the model are discussed in Appendix B. Despite this limitations, a comparison between initial model simulations and field observations is instructive, as it helps identify potential inconsistencies in the thermodynamic and kinetic data used, and areas where the conceptual model requires improvement. The following discussion addresses the degree of consistency of the mineralogical and chemical evolution of groundwater interaction with Gulf Coast sediments outside the region affected by CO_2 injection in the 1-D simulation reported in this paper. This simulation was conducted at 40 ^oC and for a 10,000 year period, and therefore differs in certain details from an earlier simulation reported in Xu et al. (2001), in Section 3.2, *Background without CO2 Injection,* which was conducted at 80 ^oC for a period of 200,000 years using some different mineral compositions. The composition of the initial aqueous phase is assumed to be an essentially pure 1.0-M solution of sodium chloride with a pH of 7 and an Eh of –0.1 V. The mineralogy of the sediment as described in this report (Table 2) represents a compromise blend of shale and sandstone in order to permit a more realistic interim representation of true conditions in the field. A comparison between model results and field observations follows for each participating mineral.

Quartz. The concentration of quartz declines slowly over the course of the simulation (Figure 16a). This behavior is inconsistent with field observations of the formation of quartz overgrowths during diagenesis due to the release of SiO_2 during replacement of smectite by illite in adjacent shales (Land, 1984). However, it should be

recognized that the simulation is essentially of the diagenesis of sandstone isolated from the enclosing shales. The proportions of reactant minerals in the simulation therefore differ from that of the total system in the field.

Kaolinite. Kaolinite destabilization (Figure 16a) over the course of the simulation in favor of illite formation (Figure 16d) is consistent with field observations in shales (Lynch, 1997). However, secondary kaolinite commonly forms in sandstones upon the decomposition of potash feldspars (Franks and Forester, 1984; Loucks et al., 1984). Thus, the simulation presents results that are inconsistent with qualitative field observations in sandstones.

Calcite. Calcite formation, resulting from the decomposition of oligoclase with the release of Ca^{2+} is consistent with field observations of Gulf Coast sandstones that have undergone diagenesis. Calcium is also released in the simulation during the conversion of smectite-Ca to smectite-Na, which normally occurs in detrital smectite prior to deposition from seawater. In the field, however, $^{87}Sr/^{86}Sr$ ratios in secondary calcite from the field suggest that the source of the Ca^{2+} was from carbonates deposited contemporaneously in adjacent shales (Milliken et al., 1981).

Illite. See K-feldspar, below.

Organic Matter. This proxy for kerogen decomposes (Figure 16b) progressively over the course of the simulation. The Eh of the system stabilizes at about -0.27 V after 6,000 years, and this results in the production of methane and the formation of small amounts of graphite (a proxy for bitumen). The rate might be somewhat higher than would be expected in a system at 40 ^{o}C. Otherwise, these results appear to be reasonable for the conditions of the simulation. A more detailed comparison with field data would

be beneficial. Further review of the decomposition kinetics of kerogen is merited, e.g., Xiao (2001), and the corollary decarboxylation as manifested by the kinetics of CO_2 release from field data (Franks and Forester, 1984).

Oligoclase. Detrital oligoclase decomposes progressively throughout the 10,000-year simulation period (Figure 16a). This behavior is broadly consistent with field observations of Gulf Coast sediments, where detrital plagioclases dissolve, to be replaced by low albite (Figure 16d).

Albite-low. Albite-low replaces oligoclase and increases in concentration progressively over the course of the simulation (Figure 16d), in qualitative agreement with field observations of diagenetic alteration in Gulf Coast sandstone aquifers. Albite-low forms through the removal of Na^+ from coexisting pore waters, although Milliken (1991) argues that not all Na^+ could be derived from this source in the field, but instead must be derived from Smectite-Na. Albite-low precipitation in the simulation also requires a source of Al (from oligoclase dissociation) and SiO_2 from the dissolution of oligoclase and detrital quartz. The latter source of silica is, however, inconsistent with field observations, where instead, excess silica is supplied from the transformation of smectite to illite in contiguous shales. The inconsistency is due to the limitation of the simulation to the diagenesis of a sandstone isolated from coexisting shales.

Smectite-Ca and Smectite-Na. Smectite-Ca (Figure 16d), decomposes progressively over the course of the simulation, which is consistent with the stabilization of smectite-Na (Figure 16d), in a 1 M solution of sodium chloride. The rate of decomposition, however, is excessively slow, indicating that the model requires provision for fast cation exchange reactions.

K-feldspar. The decomposition of K-feldspar (Figure 16a) takes place over the full simulation period (10,000 years), to be replaced by illite. This process is generally consistent with field observations at somewhat higher temperatures, i.e. approxiamtely 100 ^{o}C, where K-feldspar decomposes concurrently with smectite conversion to illite (Land, 1984).

Clinochlore. This phase (Figure 16b), is the magnesium end-member of the magnesium-ferrous iron binary solid solution, clinochlore-daphnite, and is included along with daphnite, because solid solutions cannot currently be modeled with the TOUGHREACT code. It decomposes progressively over the course of the simulation, supplying Mg^{2+} for the formation of illite. This process is generally inconsistent with field observations, where illite is observed to lose tri-octahedral Mg^{2+} during diagenesis with concomitant replacement by di-octahedral Al^{3+}, and the formation of secondary magnesian chlorite (Lynch, 1997; Lynch et al., 1997). Field observations are not simulated, because the coupled substitution of Mg for Al in illite is not presently incorporated in the thermochemical database of the TOUGHREACT code. Further refinement of the thermochemistry of illite in the simulator is justified. The source of the thermodynamic properties of clinochlore in the model is Helgeson et al. (1978). A review of more recent literature, e.g. Gottschalk (1997); Holland and Powell (1998), regarding the thermodynamic properties of clinochlore should be undertaken.

Daphnite. This phase (Figure 16b) increases slightly in concentration over the course of the simulation. The increase is at the expense of hematite, which is reduced by the organic matter.

To summarize, the simulation is partially validated by field observations of the

diagenesis of Gulf Coast sediments, and in particular, sandstones of the Frio formation of Texas. Although the current model does not entirely replicate conditions in the field, the results are generally in agreement. Further refinement of the model, the supporting thermodynamic database and kinetic data should lead to simulations that not only more accurately reflect geochemical processes that take place during diagenesis, but also enhance the capability of predicting the fate of carbon dioxide injected into deep sedimentary saline aquifers.

6. Conclusions

A reactive geochemical transport model for evaluating long-term CO_2 disposal in deep aquifers has been developed. The model has been used to analyze mineral alteration, CO_2 sequestration by secondary carbonates, and reservoir porosity changes for a Gulf Coast sediment. Sensitivity simulations have been performed by changing mineral kinetic rate constants relative to one another. Major conclusions that can be drawn are as follows:

(1) The simulation is partially validated by field observations of the diagenesis of Gulf Coast sediments, and in particular, sandstones of the Frio formation of Texas. Although the current model does not entirely replicate conditions in the field, the results are generally in agreement. Further refinement of the model, the supporting thermodynamic database and kinetic data should lead to simulations that not only more accurately reflect geochemical processes that take place during diagenesis, but also enhance the capability of predicting the fate of carbon dioxide injected into deep sedimentary saline aquifers.

(2) Variations in precipitation of secondary carbonate minerals depend on rock mineral composition and their dissolution rates. For the conditions and parameters presented in this paper, the CO_2 mineral-trapping capacity after 10,000 years is of the order of 2-5 kg per cubic meter medium, which is comparable with that of dissolution in pore waters (solubility trapping). Under favorable conditions such as increased abundance or kinetic dissolution rate constant of the Mg-bearing mineral clinochlore, the capacity may reach values

of 10 kg CO_2 per cubic meter medium. CO_2 sequestration by secondary carbonate precipitation also varies with other factors such as porosity, gas pressure, temperature, and redox condition of the deep aquifer system studied.

(3) The time needed to sequester CO_2 in mineral phases is uncertain, because mineral kinetic properties and reactive surface areas are not well constrained. In addition to the sensitivity simulations, studies on rock alteration in natural CO_2 reservoirs should be conducted to give some constrains on kinetic rates of mineral dissolution and precipitation.

(4) CO_2-induced rock mineral alteration and the addition of CO_2 mass as secondary carbonates to the solid matrix results in decreased porosity. A maximum 3% porosity decrease is obtained in our simulations. A small decrease in porosity may result in a significant decrease in permeability.

The range of problems concerning the interaction of water-CO_2-rock is very broad. The present simulation results are specific to the conditions and parameters considered. Care should be taken when extrapolating the results and conclusions for other sites. The "numerical experiments" give a detailed understanding of the dynamic evolution of a particular geochemical system. A critical evaluation of modeling results can provide useful insight into sequestration mechanisms and controlling reactive geochemical transport conditions and parameters.

Appendix A. Kinetic rate law used in the model

For kinetically-controlled mineral dissolution and precipitation, a general form of rate law (Lasaga, 1984; and Steefel and Lasaga, 1994) is used

$$r_m = A_m\, k_m \left[1 - \left(\frac{Q_m}{K_m} \right)^{\mu} \right]^n \qquad (A.1)$$

where m is mineral index, r_m is the dissolution/precipitation rate (positive values indicate dissolution, and negative values precipitation), A_m is the specific reactive surface area per kg H_2O, k_m is the rate constant (moles per unit mineral surface area and unit time) which is temperature dependent, K_m is the equilibrium constant for the mineral-water reaction written for the destruction of one mole of mineral m, and Q_m is the ion activity product, The parameters μ and n are two positive numbers normally determined by experiment, and are usually, but not always, taken equal to unity. The temperature dependence of the reaction rate constant can be expressed reasonably well via an Arrhenius equation (Lasaga, 1984; and Steefel and Lasaga, 1994). Since many rate constants are reported at 25 ^{o}C, it is convenient to approximate the rate constant dependency as a function of temperature as

$$k = k_{25} \exp\left[\frac{-E_a}{R} \left(\frac{1}{T} - \frac{1}{298.15} \right) \right] \qquad (A.2)$$

where E_a is the activation energy, k_{25} is the rate constant at 25 ^{o}C, R is the universal gas constant, and T is absolute temperature.

Appendix B. Some issues to be addressed in future modeling

The current modeling entails a number of simplifications, which limit its ability to replicate the complex patterns seen in field observations. Here we discuss a number of issues that should be addressed in future studies of diagenesis of Gulf Coast sediments.

(1) It should be recognized that the current simulations are treating the sandstone aquifer as if it were a closed system with respect to the enclosing shales. Shales are between three and twenty times as abundant as the sandstones in Gulf Coast sediments, the ratio depending on the geological formation and the proclivity of the investigator. (Galloway et al., 1982; Franks and Forester, 1984; Sharp et al., 1988). There is abundant evidence of mass transfer between clays and sandstones during diagenesis (Moncure et al., 1984; Sullivan and McBride, 1991; Milliken et al., 1994), but this process is ignored in the current model. To compensate for the lack of verisimilitude, some of the constituents of the shale have been "transferred" to the sandstone in the model, including clay minerals, organic matter, and carbonate.

(2) The current model does not adequately represent the extremely complex process of kerogen decomposition (or petroleum maturation) in deeply buried sediments. The model embodies a very simplistic representation of kerogen decomposition, thus:

$$CH_2O + O_2(g) \Rightarrow HCO_3^- + H^+$$

Which is coupled with the following equilibria:

$$C + O_2(aq) + H_2O \Leftrightarrow HCO_3^- + H^+$$

$$CO_2(aq) + H_2O \Leftrightarrow HCO_3^- + H^+$$

$$CH_4(aq) + 2O_2(g) \Leftrightarrow HCO_3^- + H^+ + H_2O$$

Kerogen, the organic matter found in sediments, particularly in shales, has a very complex structure, consisting of a tangle of aromatic and aliphatic hydrocarbon components with numerous attached oxygenated, amino, or thiol functional groups, (Tissot and Welte, 1978). As the temperature rises with burial, these groups scission sequentially, and dissolve into the aqueous phase (Hunt, 1979; Franks and Forester, 1984). The temperature range over which scission occurs in the field is from 60 to 150 ^oC. The scissioning of oxygenated groups results primarily in the production of carbonic acid, H_2CO_3, although unstable short-chain aliphatic acid anions such as acetate and butyrate also form as intermediates in what is otherwise known as decarboxylation. The maximum rate of decarboxylation occurs at about 100 ^oC (Hunt, 1979; Franks and Forester, 1984). Amino functional groups are subsequently released as the ammonium ion, NH_4^+, and finally, the thiol groups are released as HS^-. The approximate magnitude of the scissioning kinetics of these classes of functional groups can probably be estimated from laboratory studies and field investigations. The current simulations are conducted at 40 ^oC, which is below the lower temperature for decarboxylation.

(3) The progressive transformation of 2:1 clay from smectite to illite in sediments is represented in the current model only in its simplest form. A voluminous literature discussing the diagenesis of clays in sediments during progressive burial attests to the importance of this transformation as well as to its complexity. A unanimous consensus as to the mechanisms involved in this transition has not been reached within the scientific

community. However, several lines of evidence suggest the following:

- The transition is promoted by the availability of "non-exchangeable" cations such as K^+ and NH_4^+. The former is derived from the decomposition of K-feldspar, (Land, 1984; Milliken et al., 1989; Milliken, 1992; Milliken et al., 1994) which is in turn, promoted by the release of carbonic acid derived from the decarboxylation of organic matter. NH_4^+ is also released during the maturation of organic matter (Drits et al., 1997; Cuadros and Altaner, 1998; Lindgreen et al., 2000). Thus, illitization appears to be coupled with the same process that leads to the formation of petroleum. And the fact that illitization and petroleum maturation appear to reach a maximum rate at about the same temperature, circa 100 ^oC, is more than just a coincidence (Franks and Forester, 1984; Loucks et al., 1984).
- The smectite/illite transition appears to take place through several mixed intermediate phases, represented by ordered stacking sequences or polysomatic series of smectite (S) and illite (I) lamellae, such as SSSSS…., SSISSISSI…, SISISISI…, SIISIISIIS…, IIIIII…. These polysomes may in fact thermodynamically more stable than physical mixtures of illite and smectite, or randomly stacked sequences (Blanc et al., 1997). The ordered sequences therefore contribute to clay polysomatic stabilization in the field through thermodynamic rather than kinetic controls such as Ostwald rule of stages, e.g., see Primmer (1994). However, it is not clear that ordering is the only factor potentially affecting thermodynamic stabilization (see below).
- The succession of clay minerals observed during diagenesis is generally inconsistent with a simple demonstration of the Ostwald rule of stages, because experimentally observed kinetics of the smectite to illite transformation are sufficiently fast to ensure

that equilibrium would be achieved more rapidly than the rate of burial and consequent temperature increase (Eberl and Hower, 1976). Purported field evidence supporting kinetic phenomena, such as Ostwald ripening, or the Ostwald rule of stages, e.g. see Lanson and Meunier (1995) and Varajao and Meunier (1995) cannot be unambiguously ascribed to such processes without a clear demonstration that pressure and temperature remained invariant during either ripening or transformation of I/S polysomes. At least, it might be surmised that other factors are operative in sustaining thermodynamic stability or metastability apart from contributions from surface free energy and their effect on Ostwald ripening. These include variations in chemical composition or polytype (e.g., the transformation from 1Md to $2M_1$), the attachment of heterophyllic organic molecules to the clay surfaces, or other unidentified phenomena that permit stabilization, including the behavior of the electrical double layer in the aqueous phase adjacent to the clay interface, or the insertion of organic molecules in smectite during kerogen decomposition. In the context of polytype stability, the transition of illite from a lath type habit to hexagonal tabular habit, observed both in the field (Lanson and Meunier, 1995) and in the laboratory (Bauer et al., 2000) is one such example where quantification of field thermodynamic relations would be necessary before field alteration could be attributed to the Ostwald rule of stages. Another argument favoring a thermodynamic stability for the observed clay phases rather than kinetic control, is the notable reappearance of "metastable" clay minerals during retrograde metamorphism. (McDowell and Elders, 1980; Zhao et al., 1999. Also, see Rosenberg, 2002). While such occurrences are rarely reported, they strongly suggest that the observed sequence

of clay minerals during burial metamorphism is indicative of thermodynamic stability rather than kinetic control.

- The smectite of the I/S clays contains 4.5 waters in the interlayer position for every 10 lattice oxygens (Ransom and Helgeson, 1994). During illitization, this water is expelled into the pore water, and can dilute its salinity by as much as 20% (Land, 1984). The fact that formation waters more dilute than the original connate seawater, also contain aliphatic acid anions such as acetate, is suggestive that the process of kerogen breakdown and illitization are again related (Morton and Land, 1988; Macpherson, 1992; Lynch and Land, 1996).
- Illitization also leads to compositional changes in both the tetrahedral and octahedral sheets of the 2:1 clays. Al substitutes for silica in the tetrahedral sheet with the expulsion of silica. The trioctahedral Mg(II) and Fe(II) and dioctahedral Fe(III) are progressively depleted, to be replaced by dioctahedral Al (Lynch, 1997). These processes are reflected in accompanying changes in the diagenetic mineralogy. Excess silica precipitates as quartz overgrowths in adjacent sandstones, spatially removed from the locus of illitization, although retaining the oxygen isotopic signature of the source (Lynch and Land, 1996; Lynch, 1996; Lynch et al., 1997). Quartz overgrowths in sandstones constitute between 0 and 20%, but average about 2.5% of the total quartz present. Sometimes, insufficient aluminum is present in the shales to permit increased occupation of Al in both tetrahedral and octahedral sites. The deficiency is made up by removal of Al during decomposition of detrital feldspars in adjacent sandstones (Lynch et al., 1997). Note however, that Milliken et al. (1994) were unable to confirm this assumption. Otherwise, the decomposition of

kaolinite in the shales could supply aluminum with concurrent release of additional silica. Evidence for the latter process is suggested by the progressive decline in kaolinite concentration with depth in the Frio formation of Texas (Lynch, 1997). The expelled Mg is taken up through the formation of secondary magnesian chlorite (clinochlore), or sometimes through the formation of secondary dolomite or ankerite (Land, 1984; Milliken et al., 1981; Franks and Forester, 1984). The dioctahedral Fe(III) is first reduced *in situ* by the decomposing organic matter (Lynch et al., 1997), then expelled from illite and immobilized as pyrite due to the release of thiol groups during kerogen decomposition.

(4). The detrital feldspars, plagioclase and alkali feldspar, originated with the weathering of both intrusive and extrusive igneous rocks. The compositional range of both feldspars in Gulf Coast sediments is far broader than the alkali feldspar (K-feldspar) and plagioclase (oligoclase) represented in the model, (Milliken et al., 1989). While neither class of feldspar is thermodynamically stable with respect to the end members, orthoclase and low albite, both of which form during diagenesis (Loucks et al., 1984; Milliken, 1989), their relative stability is dependent in part on their chemical composition, and on other physical properties. The dissolution or replacement of detrital feldspars during diagenesis does not, therefore, follow any unique kinetic expression, but rather proceeds at rates that are dependent on their composition and that of the ambient groundwater.

(5). Interpretation of diagenetic processes within the Gulf coast sediments has been facilitated by studying the behavior of stable isotopes. Of particular, interest is the behavior of light stable isotopes represented by the variables $\delta^{18}O$, δD, $\delta^{13}C$ and $\delta^{34}S$.

These variables have been studied in both groundwaters (Franks and Forester, 1984; Fisher and Land, 1986; Morton and Land, 1988; Land, 1995; Dworkin and Land, 1996), and in coexisting diagenetic minerals, e.g. in carbonates (Franks and Forester, 1984; Fisher and Land, 1986; Lynch and Land, 1996; Lynch et al., 1997), quartz (Fisher and Land, 1986; Lynch and Land, 1996; Lynch, 1996) and kaolinite (Fisher and Land, 1986). Other stable isotopic ratios have been used to a lesser extent, such as $^{206}Pb/^{204}Pb$, $^{208}Pb/^{204}Pb$, $^{87}Sr/^{86}Sr$ and $^{11}B/^{9}B$ ratios in primary and secondary minerals and in groundwaters (Milliken et al., 1994; Land, 1995; Williams et al., 2001a,b). Isotopic systematics are not incorporated in present modeling, but model comparison with field observations would be greatly facilitated if the systematics were to be incorporated in the TOUGHREACT code.

Acknowledgements. We are grateful to Julio García for help in this work. We thank Curtis Oldenburg and Guoxiang Zhang for a review of the manuscript and suggestions for improvements. This work was supported by the Director, Office of Science, Office of Basic Energy Sciences, of the U.S. Department of Energy, under Contract No. DE-AC03-76SF00098 with Lawrence Berkeley National Laboratory.

References

Ague, J. J., and Brimhall, G. H., 1989, Geochemical modeling of steady state and chemical reaction during supergene enrichment of porphyry copper deposits, *Economic Geology*, v. 84, p. 506-528.

Apps, J. A., 1996, An approach to modeling of the chemistry of waste fluid disposal in deep saline aquifers, In Apps, J. A., and Tsang, C. F. (eds.), Deep injection disposal of hazardous and industrial waste: Scientific and Engineering Aspects, p. 465-488, Academic Press, San Diego, California.

Bachu, S., Gunter, W. D., and Perkins, E.H., 1994, Aquifer disposal of CO_2: hydrodynamic and mineral trapping, *Energy Convers. Mgmt.,* v. 35, p. 269-279.

Bauer, A., Velde, B. and Gaupp, R., 2000, Experimental constraints on illite morphology, *Clay Minerals*, v. 35, p. 587-597.

Blanc, P., Bieber, A., Fritz, B. and Duplay, J., 1997, A short range interaction model applied to illite/smectite mixed-layer minerals, *Phys. Chem. Minerals*, v. 24, p. 574-581.

Blum, A. E., and Stillings, L. L., 1995, Feldspar dissolution kinetics, Chapter 7 of chemical weathering rates of silicate minerals, White, A.F., and Brantley, S. L. (eds.), *Mineral Society of America*, v. 31, p. 291–351, Washington D. C.

Bolton, E. W., Lasaga, A. C., and Rye, D. M., 1999, Long-term flow/chemistry feedback in a porous medium with heterogenous permeability: Kinetic control of dissolution and precipitation: American Journal of Science, v. 299, p. 1-68.

Corey, A.T., 1954, The interrelation between gas and oil relative permeabilities, *Producers Monthly*, pp. 38 - 41.

Cuadros, J. and Altaner, S.P., 1998, Characterization of mixed-layer illite-smectite from bentonites using microscopic chemical, and X-ray methods: Constraints on the smectite-to-illite transformation mechanism, *American Mineralogist*, v. 83, p. 762-774.

Drits, V.A., Lindgreen, H. and Salyn, A.L., 1997, Determination of the content and distribution of fixed ammonium in illite-smectite by X-ray diffraction: Application to North Sea illite-smectite, *American Mineralogist*, v. 82, p. 79-87.

Dworkin, S.I. and Land, L.S., 1996, The origin of aqueous sulfate in Frio pore fluids and its implication for the Origin of oil field brines. *Applied Geochemistry,* vol. 11, p. 403-408.

Eberl, D. and Hower, J., 1976, Kinetics of illite formation, Geological Society of America Bulletin, v. 87, p. 1326-1330.

Folk, R.L., 1968, *Petrology of Sedimentary Rocks*, Hemphill Publishing Company, Austin, Texas, 182 pp.

Fisher, R.S. and land, L.S., 1986, Diagenetic history of Eocene Wilcox sandstones, south-central Texas. *Geochimica et Cosmochimica Acta*, v. 50, p. 551-561.

Franks, S.G. and Forester, R.W., 1984, Relationships among secondary porosity, pore fluid chemistry and carbon dioxide, Texas Gulf Coast. In *Clastic Diagenesis*, (David A. McDonald and Ronald C. Surdam, Eds.) AAG Memoir 37, Part 1, *Concepts and Principles*, p. 63-78.

Galloway, W.E., Hobday, D.K. and Magara, K., 1982, Frio Formation of Texas Gulf coastal plain-depositional systems, structural framework, and hydrocarbon distribution. *Bulletin of the American Association of Petroleum Geologists*, v. 62, p. 649-688.

García, J., Density of Aqueous Solutions of CO2, Lawrence Berkeley National Laboratory Report LBNL-49023, Berkeley, CA, 2001.

Gottschalk, M., 1997, Internally consistent data for rock-forming minerals in the system SiO_2-TiO_2-Al_2O_3-Fe_2O_3-CaO-MgO-FeO-K_2O-Na_2O-H_2O-CO_2,*European Journal of Mineralogy*, v. 9(1), p. 175-223.

Gunter W. D., Perkins, E. H., and McCann, T. J., 1993, Aquifer disposal of CO_2-rich gases: Reaction design for added capacity. *Energy Convers. Mgmt.,* v. 34, p. 941-948.

Gunter W. D., Bachu, S., Law, D. H. S., Marwaha, V., Drysdale, D. L., MacDonald, D. E., and McCann, T. J., 1996, Technical and economic feasibility of CO_2 disposal in aquifers within the Alberta Sedimentary Basin, Canada, *Energy Convers. Mgmt.* v. 37, p. 1135-1142.

Gunter W. D., Wiwchar, B., and Perkins, E. H., 1997, Aquifer disposal of CO_2-rich greenhouse gases: extension of the time scale of experiment for CO_2-sequestering reactions by geochemical modeling, *Mineral. and Petrol.*, v. 59, p. 121-140.

Helgeson, H. C., and Kirkham, D. H., 1974, Theoretical prediction of the thermodynamic behaviour of aqueous electrolytes at high pressures and temperatures: II. Debye-Hückel parameters for activity coefficients and relative partial molal properties: *American Journal of Science*, v. 274, p. 1199-1261.

Helgeson, H.C., Delany, J.M., Nesbit, H.W. and Bird, D.K., 1978, Summary and critique of the thermodynamic properties of minerals, *American Journal of Science*, v. 278A. 229 pp.

Hitchon, B. (ed.)., 1996, *Aquifer Disposal of Carbon Dioxide,* Geoscience Publishing, Ltd., Sherwood Park, Alberta, Canada.

Holland, T.J.B. and Powell, R., 1998, In internally consistent thermodynamic data set for phases of petrological interest. *Journal of Metamorphic Geology*, v. 16(3), p. 309-343.

Holloway, S., 1997, An overview of the underground disposal of carbon dioxide, *Energy Convers. Mgmt.*, v. 38, p. 193-198.

Hunt, J.M., 1972, Distribution of Carbon in the Earth's crust. *Bulletin of the American Association of Petroleum Geologists*, v.56, p. 2273-2277.

Hunt, J.M., 1979, *Petroleum Geochemistry and Geology*,W.H. Freeman and Co., San Francisco.

Johnson, J. W., Oelkers, E. H., and Helgeson, H. C., 1992, SUPCRT92: A software package for calculating the standard molal thermodynamic properties of minerals, gases, aqueous species, and reactions from 1 to 5000 bars and 0 to 1000 degrees C, *Computers and Geosciences*, v. 18, p. 899–947.

Knauss, K. G., and Wolery, T. J., 1989, Muscovite dissolution kinetics as a function of pH and time at 70°C." *Geochimica et Cosmochimica Acta,* v. 53, p. 1493–1501.

Korbol, R. and Kaddour, A., 1995, Sleipner vest CO_2 disposal - injection of removed CO_2 into the Utsira Formation, *Energy Convers. Mgmt.,* v. 36, No. 6-9, p. 509-512.

Land, L.S., 1984, Frio sandstone diagenesis, Texas Gulf Coast: A regional isotopic study. In Clastic Diagenesis, (David A. McDonald and Ronald C. Surdam, Eds.) AAG

Memoir 37, Part 1, *Concepts and Principles*, p.47-62.

Land, L.S., 1995, Na-Ca-Cl saline formation waters, Frio formation (Oligocene), South Texas, USA: Products of diagenesis. *Geochimica et Cosmochimica Acta*, v. 59(11), p. 2163-2174.

Lanson, B. and Meunier, A., 1995, The transformation of ordered (S≥1) mixed layers illite-smectite in a diagenetic series. State of the art and prospects, *Bull. Centres Rech. Explor.-Prod. Elfe Aquitain*e, v. 19(1), p. 149-165.

Lasaga, A. C., 1984, Chemical kinetics of water-rock interactions, *Journal of Geophysical Research*, v. 89, p. 4009-4025.

Law, D. H. S., and Bachu, S., 1996, Hydrogeological and numerical analysis of CO_2 disposal in deep aquifers in the Alberta Sedimentary Basin, *Energy Convers. Mgmt.,* v. 37, No. 6-8, p. 1167 - 1174.

Lindgreen, H., Drits, V.A., Sakharov, B.A., Salyn, A.L., Wrang, P. and Dainyak, L.G., 2000, Illite-smectite changes during metamorphism in black Cambrian Alum shales from the Baltic area. *American Mineralogist*, v. 85, p. 1223-1238.

Lohuis, J. A. O., 1993, Carbon dioxide disposal and sustainable development in The Netherlands, *Energy Convers. Mgmt.,* v. 34, No. 9-11, p. 815-821.

Loucks, R.G., Dodge, M.M. and Galloway, W.E., 1984, Regional controls on diagenesis and reservoir quality in Lower Tertiary sandstones along the Texas Gulf Coast. In Clastic Diagenesis, (David A. McDonald and Ronald C. Surdam, Eds.) AAG Memoir 37, Part 1, *Concepts and Principles*, p.15-45.

Lynch, F.L., 1996, Mineral/water interaction, fluid flow, and Frio sandstone diagenesis: evidence from the rocks. *Bulletin of the American Association of Petroleum Geologists,* v. 80(4), p. 486-504.

Lynch, F.L., 1997, Frio shale mineralogy and the stoichiometry of the smectite-to-illite reaction: the most important Reaction in clastic sedimentary diagenesis. *Clays and Clay Minerals*, v. 45(5), p. 618-631.

Lynch, F.L. and Land, L.S., 1996, Diagenesis of calcite cement in Frio formation sandstones and its relationship to formation water chemistry. *Journal of Sedimentary Research*, v. 66 (3), p. 439-446.

Lynch, F.L., Mack, L.E. and Land, L.S., 1997, Burial diagenesis of illite/smectite in

shales and the origins of authigenic quartz and secondary porosity in sandstones. *Geochimica et Cosmochimica Acta*, v. 61(10), p. 1995-2006.

Macpherson, C.L, 1992, Regional variations in formation water chemistry: Major and minor elements, Frio formation fluids, Texas. *Bulletin of the American Association of Petroleum Geologists,* v. 76(5), p. 740-757.

McDowell, S.D. and Elders, W.A., 1980, Authigenic silicates in borehole Elmer, 1, Salton Sea geothermal field, California, U.S.A, *Contributions to Mineralogy and Petrology*, v. 74, p. 293-310.

Milliken, K.L., McBride, E.F. and Land, L.S., 1989, Numerical assessment of dissolution versus replacement in the subsurface destruction of detrital feldspars, Oligocene Frio formation, south Texas. *Journal of Sedimentary Petrology*, v. 59(5), p. 740-757.

Milliken, K.L, 1989, Petrography and composition of authigenic feldspars, Oligocene Frio formation, south Texas. *Journal of Sedimentary Petrology*, vol. 59(5), p. 361-374.

Milliken, K.L., 1992, Chemical behavior of detrital feldspars in mudrocks versus sandstones, Frio formation (Oligocene), south Texas. *Journal of Sedimentary Petrology*, vol. 62(9), p. 790-801.

Milliken, K.L., Land, L.S. and Loucks, R.G., 1981, History and burial diagenesis determined from isotopic geochemistry, Frio formation, Brazoria County, Texas, Bulletin of the American Association of Petroleum Geologists, v. 65, p. 1397-1413.

Milliken, K.L, Mack, L.E. and Land, L.S., 1994, Elemental mobility in sandstones during burial: Whole rock chemical and Isotopic data, Frio formation, south Texas. *Journal of Sedimentary Research*, v. A64(4), p. 788-796.

Moncure, G.K., Lahann, R.W. and Siebert, R.M., 1984, Origin of secondary porosity and cement distribution in a sandstone/shale sequence from the Frio formation (Oligocene). In *Clastic Diagenesis* (D.A. McDonald and R.C. Surdam, Eds), American Association of Petroleum Geologists Memoir 37, p. 151-161.

Morton, R.A. and Land, L.S., 1988, Regional variations in formation water chemistry, Frio Formation (Oligocene), Texas Gulf Coast: Reply. *Bulletin of the American Association of Petroleum Geologists*, v. 72(7), p. 858-859.

Nagy, K. L., Dissolution and precipitation kinetics of sheet silicates, 1995, *Chemical Weathering Rates of Silicate Minerals,* v. 31, p. 291–351.

Narasimhan, T. N., and Witherspoon, P. A., 1976, An integrated finite difference method for analyzing fluid flow in porous media, *Water Resources Research*, v. 12, p. 57–64.

Nordstrom, D. K., Alpers, C. N., 1997, The Environmental geochemistry of mineral deposits. Part A. Processes, methods and health Issues. (Plumlee, G. S., Logsdon, M. J. (Eds)): Reviews in Economic Geology, v. 6**,** Society of Economic Geologists.

Nordstrom, D. K., and Muñoz, J. L., 1986, *Geochemical Thermodynamics*, The Benjamin/Cummings Pub. Co., Menlo Park, California, 477 p.

Ortoleva, P. J., Dove, P., and Richter, F., 1998, Geochemical perspectives on CO_2 sequestration, Manuscript prepared for U. S. Department of Energy Workshop on "Terrestrial Sequestration of CO_2 - An Assessment of Research Needs," Gaithersburg, MD, May 10 - 12.

Parkhurst, D. L., Thorstenson, D. C., and Plummer, L. N., 1980, PHREEQE: A computer program for geochemical calculations: US Geological Survey, Water Resources Investigation 80-96, 174 p.

Pearce, J. M., Holloway, S., Wacker, H., Nelis, M. K., Rochelle, C., and Bateman, K., 1996, Natural occurrences as analogues for the geological disposal of carbon dioxide. *Energy Convers. Mgmt.,* v. 37 (6-8), p. 1123-1128.

Perkins, E.H. and Gunter, W.D., Mineral Traps for Carbon Dioxide, in: B. Hitchon (ed.), *Aquifer Disposal of Carbon Dioxide*, Geoscience Publishing, Ltd., Alberta, Canada, pp. 93 - 113, 1996.

Plummer, L. N., Wigley, T. M., and Parkhurst, D. L., 1978, The kinetics of calcite dissolution in CO_2 systems at 5ºC to 60ºC and 0.0 to 1.0 atm CO_2, *American Journal of Science*, v. 278, p. 179-216.

Primmer, T.J., 1994, Some comments on the chemistry and stability of interstratified illite-smectite and the role of Ostwald-type processes, *Clay Minerals*, v. 29, p. 63-68.

Pruess, K., 1991, TOUGH2: A general numerical simulator for multiphase fluid and heat flow: Lawrence Berkeley Laboratory Report LBL-29400, Berkeley, California.

Pruess, K., Oldenburg, C., and Moridis, G., 1999, TOUGH2 user's guide, Version 2.0, Lawrence Berkeley Laboratory Report LBL-43134, Berkeley, California.

Pruess, K., and García, J., 2001, Multiphase flow dynamics during CO2 disposal into saline aquifers, Submitted to Environmental Geology.

Pruess, K., Xu, T., Apps, J., and García, J., February 2001, Numerical Modeling of Aquifer Disposal of CO2, Paper SPE-66537, presented at SPE/EPA/DOE Exploration and Production Environmental Conference, San Antonio, TX, USA.

Ransom, B. and Helgeson, H.C., 1994, A chemical and thermodynamic model of the aluminous 2:1 dioctahedral layer clay minerals in diagenetic processes: Regular solution model of the interlayer dehydration in smectite, *American Journal of Science*, v. 294, p. 449-484.

Reed, M. H., 1982, Calculation of multicomponent chemical equilibria and reaction processes in systems involving minerals, gases and aqueous phase, *Geochimica et Cosmochimica Acta*, v. 46, p. 513-528.

Rochelle, C. A., Bateman, K., and Pearce, J. M., 1996, Fluid-rock interactions resulting from the underground disposal of carbon dioxide, In Bottrell, S. H. (ed.), Proc., 4th lnt. Symp. Geochem, Earth's Surf., University of Leeds, Dep. of Earth Sciences, Leeds, UK., p. 448-452.

Rosenberg, P.E., 2002, The nature, formation, and stability of end-member illite: A hypothesis, *American Mineralogist*, v. 87, p. 103-107.

Rosenberg, P.E., Kittrick, J.A. and Aja, S.U., 1990, The stability of illite/smectite during diagenesis: A multiphase model, *American Mineralogist*, v. 75, p. 1182-1185.

Rudnicki, J. I., and Wawersik, W. R., 1999, Report looks at sequestering CO_2 beneath earth's surface, EOS, Transactions of American Geophysical Union, v. 80, No. 50, p. 607-608.

Sharp, J.M., Jr., Galloway, W.E., Land, L.S., McBride, E.F., Blanchard, P.E., Bodner, D.P., Dutton, S.P., Farr, M.R., Gold, P.B., Jackson, T.J., Lundegard, P.D., Macpherson, G.L. and Milliken, K.L., 1988, Diagenetic processes in Northwestern Gulf of Mexico sediments. In *Developments in Sedimentology*, v. 43, Diagenesis II (G.V. Chilingarian and K.H. Wolf, Eds). Elsevier, New York, p. 43-113.

Steefel, C. I., and van Cappellen, P., 1990, A new kinetic approach to modeling water-rock interaction: The role of nucleation, precursors and Ostwald ripening, *Geochimica Cosmochimica Acta*, v. 54, p. 2657-2677.

Steefel, C. I., and Lasaga, A. C., 1994, A coupled model for transport of multiple chemical species and kinetic precipitation/dissolution reactions with applications to reactive flow in single phase hydrothermal system, *American Journal of Science*, v. 294, p. 529-592.

Sullivan, K.B. and McBride, E.F., 1991, Diagenesis of sandstones at shale contacts and diagenetic heterogeneity, Frio formation, Texas. *Bulletin of the American Association of Petroleum Geologists*, v. 75, p. 121-138.

Svensson, U. and Dreybrodt, W., 1992. Dissolution kinetics of natural calcite minerals in CO_2-water systems approaching calcite equilibrium." *Chemical Geology*, v. 100, p. 129–145. Amsterdam, The Netherlands, Elsevier Science Publishers.

Tempel, R.N. and Harrison, W.J., 2000, Simulation of burial diagenesis in the Eocene Wilcox Group of the Gulf of Mexico basin. *Applied Geochemistry,* v.15, p.1071-1083.

Tester, J. W., Worley, G. W., Robinson, B. A., Grigsby, C. O., and Feerer, J. L., 1994, Correlating quartz dissolution kinetics in pure water from 25° to 625 °C., *Geochimica et Cosmochimica Acta*, v. 58, p. 2407–2420.

Tissot, B.P. and Welte, D.H., 1978, *Petroleum Formation and Occurrence: A New Approach to Oil and Gas Exploration*. .Springer Verlag, New York, 538 p.

van Genuchten, M.Th., 1980, A Closed-form equation for predicting the hydraulic conductivity of unsaturated soils, *Soil Sci. Soc. Am. J.*, Vol. 44, pp. 892 - 898.

Varajao, A. and Meunier, A., 1995, Particle morphological evolution during the conversion of I/S to illite in Lower Cretaceous shales from Sergipe-Alagao basin, Brazil, *Clays and Clay minerals*, v. 43(1), p. 14-28.

Verma, A., and Pruess, K., 1988, Thermohydrological conditions and silica redistribution near high-level nuclear wastes emplaced in saturated geological formations: Journal and Geophysical Research, v. 93, p. 1159-1173.

Walter, A. L., Frind, E. O., Blowes, D. W., Ptacek, C. J., and Molson, J. W., 1994, Modeling of multicomponent reactive transport in groundwater, 1, Model development and evaluation, Water Resource Research, v. 30, p. 3137-3148.\

Weir, G.J., S.P. White and W.M. Kissling, Reservoir Storage and Containment of Greenhouse Gases, in: K. Pruess (ed.), *Proceedings of the TOUGH Workshop '95*,

Lawrence Berkeley National Laboratory Report LBL-37200, pp. 233 - 238, Berkeley, CA, 1995.

White, A. F., and Peterson, M. L., 1990, Role of reactive surface area characterization in geochemical models, In Chemical Models of Aqueous Systems 2, Amer. Chem. Soc. Symp. Ser., 461-475.

Williams, L.B., Hervig, R.L., Holloway, J.R. and Hutcheon, I., 2001a, Boron chemistry during diagenesis. Part I. Experimental determination of fractionation during illitization of smectite. *Geochimica et Cosmochimica Acta*, v. 65(11), p. 1769-1782.

Williams, L.B., Hervig, R.L. and Hutcheon, I., 2001b, Boron chemistry during diagenesis. Part II. Application to organic-rich sediments. *Geochimica et Cosmochimica Acta*, v. 65(11), p. 1769-1782.

Wolery, T. J., 1992, EQ3/6: Software package for geochemical modeling of aqueous systems: Package overview and installation guide (version 7.0), Lawrence Livermore National Laboratory Report UCRL-MA-110662 PT I, Livermore, California.

Xiao, Y., 2001, Modeling the kinetics and mechanisms of petroleum and natural gas generation: A first principles approach. Molecular Modeling Theory :Applications in the Geosciences (R.T. Cygan and J.D. Kubicki, Eds) *Reviews in Mineralogy and Geochemistry*, v. 42, p. 383-436, Mineralogical Society of America, Washington, DC.

Xu, T., and Pruess, K., 1998, Coupled modeling of non-isothermal multiphase flow, solute transport and reactive chemistry in porous and fractured media: 1. Model development and validation: Lawrence Berkeley National Laboratory Report LBNL-42050, Berkeley, California, 38 p.

Xu T., Apps, J., and Pruess, K., 2001, Analysis of mineral trapping for CO_2 disposal in deep aquifers, Lawrence Berkeley National Laboratory Report LBNL-46992, Berkeley, California, 104 pp.

Xu, T., and K. Pruess, 2001, Modeling multiphase non-isothermal fluid flow and reactive geochemical transport in variably saturated fractured rocks: 1. Methodology, *American Journal of Science*, v. 301, p. 16-33.

Yeh, G. T., and Tripathi, V. S., 1991, A model for simulating transport of reactive multispecies components: model development and demonstration, *Water Resources Research*, v. 27, p. 3075-3094.

Zhao, G., Peacor, D.R. and McDowell, S.D., 1999, “Retrograde diagenesis” of clay minerals in the Precambrian Freda Sandstone, Wisconsin, *Clays and Clay Minerals*, v. 47(2), p. 119-130.